Part I :

THE LARGE-SCALE DYNAMICS OF SOLAR WIND

Paul Charbonneau

HAO/NCAR (FL2, room 3022)

tel. 497-1594

email: paulchar@hao.ucar.edu

1. STATIC CORONA MODELS

"...to the scientist it is a constant source of wonder that Nature has created its highest works without ever violating its own laws."

Konrad Lorenz
On Aggression (1963)

This section starts off with a brief presentation of the relevant equations that we will encounter in building models for the solar corona and wind (§1.1). A brief look at their range of validity is taken in §1.2. The real work begins in §1.3, where some alternatives to using the full energy equation are discussed. Finally, various classes of static corona models are constructed and critically discussed in §1.4.

1.1 Governing equations

Even though things may usually look smooth and continuous at our macroscopic level, matter is fundamentally discrete in nature. A description of the motion of any large scale body (solid, liquid or gaseous) could thus, in principle, be reconstructed by applying the laws of mechanics to every one of the body's discrete constituent. This would simply fall under the class of N-body problems, but N would be ridiculously large: the motion of $1\,\mathrm{cm}^3$ of air at room pressure and temperature would involve tracking the motions of $\sim 10^{20}$ particles, each interacting with the others. Even if this were computationally feasible, we also face the problem of specifying meaningful initial conditions for the system.

But the very fact that we are dealing with a large number of particles means that the system may be amenable to statistical treatment. Define a distribution function $f(\mathbf{x}, \mathbf{v}, t)$ such that the quantity $f\,\mathrm{d}^3\mathrm{x}\mathrm{d}^3\mathrm{v}$ corresponds to the number of particles in a 6-D volume element in phase space centered on $(\mathbf{x}, \mathbf{v})$ at time t. Macroscopic field variables, for example the density, can be constructed by constructing suitable *moments* of this distribution:

$$\rho(\mathbf{x}, t) = \int m f(\mathbf{x}, \mathbf{v}, t)\,\mathrm{d}^3\mathrm{v} \tag{1.1}$$

(where we have assumed that all particles are identical and have mass m). Clearly, the time evolution of macroscopic field variables can be reconstructed provided that the time-evolution of f is known. The latter is governed by the *Boltzmann equation*:

$$\frac{\partial f}{\partial t} + \mathbf{v} \cdot \frac{\partial f}{\partial \mathbf{x}} - \frac{\partial V}{\partial \mathbf{x}} \frac{\partial f}{\partial \mathbf{v}} = \left(\frac{\partial f}{\partial t} \right)_c . \tag{1.2}$$

The second term on the LHS corresponds to the variation in f due to particles moving around "slowly" in the $\mathbf{x}$ part of phase space, and the third term on the RHS to particles moving around "slowly" in the $\mathbf{v}$ part of phase space due to the action of smoothly varying background body forces (e.g. gravity), the action of which is represented by the potential V. The term on the RHS corresponds to variations due to particle appearing "suddenly" at a given point in phase space as a consequence of a sudden change in momentum due to a collision with another particle. Note that the above form of the Boltzmann equation is valid only for non-relativistic motions. Taking successive moments of the Boltzmann equations [as in eq. (1.1)] yields the familiar equations of conservation of mass, momentum, and energy:

$$\frac{\mathrm{D}\rho}{\mathrm{D}t} + \rho \nabla \cdot \mathbf{v} = 0, \tag{1.3}$$

$$\rho \frac{\mathrm{D}\mathbf{v}}{\mathrm{D}t} = -\rho \nabla V - \nabla p + \nabla \cdot \tau, \tag{1.4}$$

$$\rho \, c_v \frac{\mathrm{D}T}{\mathrm{D}t} + p \nabla \cdot \mathbf{v} = \nabla \cdot (\chi \nabla T) + \Psi(\mathbf{v}), \tag{1.5}$$

where $D/Dt = \partial/\partial t + \mathbf{v} \cdot \nabla$, c_v the (constant) specific heat at constant volume, χ the coefficient of heat conduction, and Ψ is a source term corresponding to energy dissipation due to viscosity[1]. The quantity τ is the viscous stress tensor, whose components, for a Newtonian fluid, are expressed as

$$\tau_{ij} = \mu \left(\frac{\partial v_i}{\partial x_j} + \frac{\partial v_j}{\partial x_i} - \frac{2}{3} \delta_{ij} \frac{\partial v_k}{\partial x_k} \right) + \mu_\theta \delta_{ij} \frac{\partial v_k}{\partial x_k} \tag{1.6}$$

where μ is the coefficient of shear viscosity, μ_θ the coefficient of bulk viscosity, and summation on repeated indices applies. Equations (1.3) through (1.6) now describe the time-evolution of *macroscopic* field quantities (ρ, $\mathbf{v}$, etc.). By introducing the

[1] Equation (1.5) may not be the form of the energy equation that you are most familiar with, and is not actually the form one obtains upon taking the second moment of Boltzmannn's equation. Using the first and second laws of themodynamics, the energy equation can be alternately written in term of changes of entropy ($\mathrm{D}S/\mathrm{D}t = ...$), of internal energy ($\mathrm{D}U/\mathrm{D}t = ...$), etc. The form given in eq. (1.5) is just the most convenient for our purposes. One thing to note, however, is that eq. (1.5) does not contain terms associated with the transport of energy by radiation, and is thus only applicable to non-radiating fluids. When dealing with radiating fluids, extra terms appear on the RHS of both the momentum and energy equations.

notion of distribution function we have gone from a N-body description to a 6-D+time description in f, and by taking moments of Boltzmann's equation to a 3-D+time description in macroscopic field quantities. The point is that the procedure rests on the assumption that a meaningful distribution function can be constructed. This, typically, is the case if each cell in phase space is well populated. We should always keep this in mind, especially when we use equations (1.3), (1.4) and (1.5) to describe the macroscopic behavior of a low density system.

In the presence of moving electrical charges, we also have to deal with electric and magnetic fields pervading the plasma. Their behavior is governed by Maxwell's equations:

$$\nabla \cdot \mathbf{E} = 4\pi\rho_e, \tag{1.7}$$

$$\nabla \times \mathbf{E} = -\frac{1}{c}\frac{\partial \mathbf{B}}{\partial t}, \tag{1.8}$$

$$\nabla \cdot \mathbf{B} = 0, \tag{1.9}$$

$$\nabla \times \mathbf{B} = \frac{4\pi}{c}\mathbf{j}_e + \frac{1}{c}\frac{\partial \mathbf{E}}{\partial t}, \tag{1.10}$$

where ρ_e is the local charge density and $\mathbf{j}_e$ is the conduction current. We must also introduce in the equations of motion (1.4) a term proportional to the Lorentz Force[2]

$$\mathbf{F} \propto \mathbf{E} + \frac{\mathbf{v}}{c} \times \mathbf{B},$$

describing the influence of the electromagnetic field on moving electrical charges. The *magnetohydrodynamic limit* is that in which

- The plasma is assumed to be electrically neutral on all relevant macroscopic scales ($\rho_e = 0$),
- The conduction current dominates over the displacement current in (1.10),
- The conduction current is proportional to the local electric field (Ohm's law),
- Plasma motions are non-relativistic.

Under these circumstances (and assuming a *scalar* electrical conductivity σ_e), Maxwell's equations can be manipulated to yield the *induction equation*:

$$\frac{\partial \mathbf{B}}{\partial t} = \nabla \times (\mathbf{v} \times \mathbf{B}) - \nabla \times (\eta \nabla \times \mathbf{B}), \tag{1.11}$$

where $\eta = c^2/4\pi\sigma_e$ is the *magnetic diffusivity*, and the Lorentz Force assumes the form

$$\mathbf{F} = \frac{1}{4\pi}(\nabla \times \mathbf{B}) \times \mathbf{B} \tag{1.12}$$

so that the equation of motion becomes

$$\rho\frac{\mathrm{D}\mathbf{v}}{\mathrm{D}t} = -\rho\nabla V - \nabla p + \frac{1}{4\pi}(\nabla \times \mathbf{B}) \times \mathbf{B} + \nabla \cdot \tau, \tag{1.13}$$

[2] Do you recall what the proportionality constant is?

The evolution of the system is then described by eqs. (1.3), (1.5), (1.11) and (1.13)[3]. Lets look back at these equations. Equation (1.11) and (1.13) are in fact each three equations, one for each vector component of $\mathbf{v}$ and $\mathbf{B}$. Together with eqs. (1.3) and (1.5), this makes eight equations. But we have *nine* field variables: in spherical polar coordinates, v_r, v_θ, v_ϕ, ρ, p, T, B_r, B_θ, and B_ϕ. We need an extra equation to complete the system (the mathematical expression for this is *closure*). The extra equation needed is the *equation of state*, which we write for now as

$$p = f(\rho, T, ...). \tag{1.14}$$

You are already familiar with the equation of state for a perfect gas, $p = NkT = \rho kT/\mu m$. We now have as many equations as unknown, and can thus proceed[4,5]. In this and following chapters, all coronal and wind models are constructed within the framework of non-radiating, single fluid, ideal hydrodynamics and magnetohydrodynamics. "Ideal" in this context refers to the neglect of dissipative processes ($\tau = 0$ in eq. [1.13], and $\eta = 0$ in [1.11]). We further assume that our single fluid behaves like a *perfect gas*, with constituents having a mass μm, where m is the proton mass and μ the mean molecular weight ($= 1/2$ for fully ionized Hydrogen). We also neglect self-gravity of the coronal gas, so that gravity becomes a given function of heliocentric radius.

For future reference, here are the three components of the equations of motion

---

[3] When magnetic fields (and thus electric currents) are present, an additional source-like term also appears on the RHS of the energy equation, corresponding to the energy liberated by the resistive dissipation of electric currents:

$$S_B \propto \frac{c^2}{(4\pi)^2 \sigma_e} ||\nabla \times \mathbf{B}||^2.$$

This extra term is negligible in all applications considered in these notes. However, evidence is mounting that it plays an important role in coronal heating.

[4] Hey, what about $\nabla \cdot \mathbf{B} = 0$?? This is one of Maxwell's equation, expressing the conservation of magnetic flux. Yet if we specify it in addition to eqs. (1.11) we end up with more equations than unknowns, which corresponds to an overspecified system of equations. After all, eqs. (1.11) described the *time-evolution* of $\mathbf{B}$, while $\nabla \cdot \mathbf{B} = 0$ needs to be satisfied whether $\mathbf{B}$ is evolving or not. Can we consider that the constraint $\nabla \cdot \mathbf{B} = 0$ is truly "built in" eqs. (1.11)?

[5] We actually need more information regarding the *composition* of the gas. In what follows, we will almost exclusively consider a globally neutral electron-proton gas, i.e., fully ionized hydrogen. We will implicitly assume that proton-electron collisions always redistribute energy between the two constituents. Consequently, we can use a *single fluid* description, where a gas "particle" is electrically neutral and has a mass equal to half the proton mass. Models that explicitely treat electrons and protons as two distinct components are called *two-fluid* models.

in standard spherical coordinates (r, θ, ϕ):

$$\rho\left(\frac{\mathrm{D}v_r}{\mathrm{D}t} - \frac{v_\theta^2 + v_\phi^2}{r}\right) = -\rho\frac{\partial V}{\partial r} - \frac{\partial p}{\partial r}$$

$$+\frac{B_\phi}{r\sin\theta}\left[\frac{\partial B_r}{\partial\phi} - \frac{\partial}{\partial r}(rB_\phi\sin\theta)\right] - \frac{B_\theta}{r}\left[\frac{\partial}{\partial r}(rB_\theta) - \frac{\partial B_r}{\partial\theta}\right], \tag{1.15}$$

$$\rho\left(\frac{\mathrm{D}v_\theta}{\mathrm{D}t} + \frac{v_r v_\theta}{r} - \frac{v_\phi^2\cot\theta}{r}\right) = -\frac{\rho}{r}\frac{\partial V}{\partial\theta} - \frac{1}{r}\frac{\partial p}{\partial\theta}$$

$$-\frac{B_\phi}{r\sin\theta}\left[\frac{\partial}{\partial\theta}(B_\phi\sin\theta) - \frac{\partial B_\theta}{\partial\phi}\right] + \frac{B_r}{r}\left[\frac{\partial}{\partial r}(rB_\theta) - \frac{\partial B_r}{\partial\theta}\right], \tag{1.16}$$

$$\rho\left(\frac{\mathrm{D}v_\phi}{\mathrm{D}t} + \frac{v_r v_\phi}{r} + \frac{v_\theta v_\phi\cot\theta}{r}\right) = -\frac{\rho}{r\sin\theta}\frac{\partial V}{\partial\phi} - \frac{1}{r\sin\theta}\frac{\partial p}{\partial\phi}$$

$$+\frac{B_\theta}{r\sin\theta}\left[\frac{\partial}{\partial\theta}(B_\phi\sin\theta) - \frac{\partial B_\theta}{\partial\phi}\right] - \frac{B_r}{r\sin\theta}\left[\frac{\partial B_r}{\partial\phi} - \frac{\partial}{\partial r}(rB_\phi\sin\theta)\right], \tag{1.17}$$

Note also that in spherical geometry, the gradient, divergence, and curl operators take the following form:

$$\nabla f = \frac{\partial f}{\partial r}\hat{\mathbf{e}}_r + \frac{1}{r}\frac{\partial f}{\partial\theta}\hat{\mathbf{e}}_\theta + \frac{1}{r\,\sin\theta}\frac{\partial f}{\partial\phi}\hat{\mathbf{e}}_\phi, \tag{1.18}$$

$$\nabla\cdot\mathbf{A} = \frac{1}{r^2}\frac{\partial}{\partial r}(r^2 A_r) + \frac{1}{r\,\sin\theta}\frac{\partial}{\partial\theta}(A_\theta\sin\theta) + \frac{1}{r\,\sin\theta}\frac{\partial A_\phi}{\partial\phi}, \tag{1.19}$$

$$\nabla\times\mathbf{A} = \frac{1}{r\,\sin\theta}\left[\frac{\partial}{\partial\theta}(A_\phi\sin\theta) - \frac{\partial A_\theta}{\partial\phi}\right]\hat{\mathbf{e}}_r$$

$$+\frac{1}{r\,\sin\theta}\left[\frac{\partial A_r}{\partial\phi} - \frac{\partial}{\partial r}(r\,A_\phi\sin\theta)\right]\hat{\mathbf{e}}_\theta + \frac{1}{r}\left[\frac{\partial}{\partial r}(r\,A_\theta) - \frac{\partial A_r}{\partial\theta}\right]\hat{\mathbf{e}}_\phi. \tag{1.20}$$

1.2 Some comments on the range of validity of the MHD equations

Central to the differential equations listed in the preceeding section is the concept of *infinitesimal volume element*. This is a region of space small enough that field variables (ρ, T, $\mathbf{U}$, etc) are approximately constant within the element, constant in the sense that *stochastic* fluctuations around the mean are extremely small.

Consider the field variable we call density. By definition, it is simply

$$\rho = \frac{\mathrm{dM}}{\mathrm{dV}}, \tag{1.21}$$

where dM is the mass contained in the volume element dV. But we know that at the microscopic level our fluid is made up of individual discrete atoms (or molecules or whatever). Therefore, reverting to a microscopic description we should rather write

$$\rho = \frac{1}{\mathrm{dV}} \sum_{i=1}^{n} m_i, \tag{1.22}$$

where m_i is the mass of particle i and n is the total number of particle present in our volume element dV. Now even though we may be dealing with a system which is, at the macroscopic level, in a steady-state ($\partial/\partial t = 0$ for all field variables), we know that at the macroscopic level the particulate constituents are not at rest; in a system in thermodynamic equilibrium at temperature T, the average constituent speed is

$$\bar{v} = \sqrt{\frac{3kT}{m}}, \tag{1.23}$$

where k is Boltzmann's constant. This means that over a time interval τ, some particles are likely to cross the boundary of dV (either inward or outward). This means that in eq. (1.22), we should have the sum running over $n(t)$. Clearly for eqs. (1.21) and (1.22) to be equivalent n must be approximately constant in time. Under what conditions does is this condition satisfied? Recalling what was said in §1.1, it is clear that the answer to this question involves something like evaluating the temporal fluctuations in $f(\mathbf{x}, \mathbf{v})$ at constant $\mathbf{x}$. This lies squarely in the realm of statistical mechanics, and any detailed treatment would take us far astray from our subject matter (see however the references at the end of this section).

It is still possible to obtain an intuitive feel for the magnitude of these fluctuations. Statistically, we can expect that for an additive quantity q "tagged" on discrete particles (e.g. mass or electric charge), relative fluctuations ($\delta q/q$) around the mean in a fixed volume are expected to vary as $1/\sqrt{n}$, where n is the total number of particles in the volume. This again tell us that the fluid description will run into trouble if our system contains relatively few particle, i.e., in the low density limit. But lets try to be a bit more physical. It should not be hard to convince yourself that fluctuations will remain small as long as our volume element has linear dimensions much larger than the typical mean free path (λ) of particles between collision. If that is the case, then most particles in dV will be doing a form of random walk *within* dV, with very few particles actually crossing the boundaries of dV. For fully ionized hydrogen, the mean free path is approximately given by

$$\lambda = \bar{v} t_C, \tag{1.24}$$

where t_C is the time required for a particle to "accumulate" a 90^o deflection via coulomb scattering:

$$t_C \simeq 3 \times 10^{-12} \frac{\bar{v}^3}{N \, \ln \Lambda}, \qquad [\mathrm{s}], \tag{1.25}$$

where in this latter expression we have

$$\Lambda = 1.24 \times 10^4 \frac{T^{3/2}}{N^{1/2}}. \tag{1.26}$$

It turns out that $\ln \Lambda \simeq 22$ is an excellent approximation over the range of temperatures and densities that we will encounter in the corona. For conditions typical of the corona ($T = 10^6$ K, $N = 10^8 \, \mathrm{cm}^3$), we have $\bar{v} \simeq 150 \, \mathrm{km \, s^{-1}}$, and $\lambda \simeq 700$ km. The pressure scale height, in turn, is $H = kT/\mu m g \sim 10^5$ km. Clearly, we are in the regime $\lambda \ll H$, and the fluid approximation is valid in describing coronal gas. At the earth's orbit, however, we have $T \sim 10^5$ K and $N \sim 10^2 \, \mathrm{cm}^3$, yielding $\lambda \sim 6 \times 10^6$ km !!

Does this mean that our fluid description is invalid in describing the flow of interplaneraty plasma around the earth? The answer is: sometimes ! As long as we are interested in bulk, large-scale flow properties such as streaming velocity, mass flux, etc., the fluid equations turn out to do a pretty good job. For other things such as the interaction of interplanetary gas with the earth's magnetic field, for example, they are sometimes limited in applicability.

Another concept that we have encountered (admittedly briefly) in manipulating Maxwell's equations into the induction equation (1.11) is that of local electric charge neutrality. This holds down to the Debye length:

$$\ell_D = \sqrt{\frac{kT}{4\pi N e^2}}. \tag{1.27}$$

Again for $T = 10^6$ K and $N = 10^8 \, \mathrm{cm}^3$, we have $\ell_D \sim 1$ cm, while for $T = 10^5$ K and $N = 10^2 \, \mathrm{cm}^3$, $\ell_D \sim 2$ m. In both cases, this is well below the relevant length scales for field quantities.

1.3 A thermodynamic divertion: polytropic and isothermal flows

Even for relatively simple geometries and magnetic field configurations, the system of equations defined by eqs. (1.1) through (1.5) is frightfully complex. One avenue of simplification that will be used extensively in the following sections consists in solving for the *dynamics* of the flow while making some rather drastic assumptions regarding the *energetics* of the flow. In simpler terms, to get rid of the energy equation. But if we do choose to omit the energy equation from our system, we must introduce another relation between some of our system variables in order to still have as many equations as unknown field variables.

The starting point of our discussion is the assumption that at every point in the flow, there exists a *linear* relationship between fractional variations of pressure and density:

$$\frac{\mathrm{d}p}{p} = \alpha \frac{\mathrm{d}\rho}{\rho}; \tag{1.28}$$

or, equivalently,

$$\frac{\mathrm{d}\ln p}{\mathrm{d}\ln \rho} = \alpha. \tag{1.13}$$

This integrates directly to

$$p = p_0 \left(\frac{\rho}{\rho_0}\right)^{\alpha}, \tag{1.14}$$

which fully specifies the pressure field in terms of the density profile. What does this assumption correspond to physically ? Using the equation of state for a perfect gas, it is easy to show that

$$\frac{\mathrm{d}\ln\, p}{\mathrm{d}\ln\, \rho} = \left(1 + \frac{\mathrm{d}\ln T}{\mathrm{d}\ln \rho}\right). \tag{1.15}$$

Since the specific volume V is simply ρ^{-1}, this expression can be rewritten as

$$\frac{\mathrm{d}\ln\, p}{\mathrm{d}\ln\, \rho} = \left(1 - \frac{c_p - c_v}{p}\frac{\mathrm{d}T}{\mathrm{d}V}\right), \tag{1.16}$$

where we made use of Carnot's Law, $R = c_p - c_v$, which relates the gas constant ($R = k/\mu m$) and the specific heats at constant pressure (c_p) and volume (c_v). Clearly, α is related to the thermodynamic properties of the gas. The second law of thermodynamics is

$$\mathrm{d}Q = \mathrm{d}U + p\mathrm{d}V. \tag{1.17}$$

This simply says that any local heat input ($\mathrm{d}Q$) goes either into increasing the specific energy of the gas ($\mathrm{d}U$) or expansion work against the ambiant pressure ($p\mathrm{d}V$). From a macroscopic standpoint, the *specific heat* (C) is defined via the relation

$$\mathrm{d}Q = C\mathrm{d}T, \tag{1.18}$$

and gives a measure of the amount of heating/cooling per unit mass required to produce a net temperature change of magnitude $\mathrm{d}T$[6]. Furthermore, we also have

$$\mathrm{d}U = c_v\mathrm{d}T, \tag{1.19}$$

[6] This, incidentally, is the basis on which the first quantitatively significant measurement of the *solar constant* was carried out; In 1837, Herschel (yes the same discoverer of Uranus and proponent of the sunspot-as-holes-in-the Sun theory) did so using an *actinometer* (basically a bowl of water with a thermometer in it). The actinometer is exposed to the Sun for a specific period of time, and the temperature rise measured. With the specific heat of water an experimentally determined quantity, the heat output can be determined directly from eq. (1.18). Herschel obtained a value of about half the modern, accepted value of 1.388×10^6 erg cm^{-2} s^{-1}. Any idea why that may have been so ?

Using these two expression, the second law can be manipulated to yield

$$\frac{\mathrm{d}V}{\mathrm{d}T} = \frac{C - c_v}{p}. \tag{1.20}$$

Equation (1.15) then becomes

$$\frac{\mathrm{d}\ln p}{\mathrm{d}\ln \rho} = \frac{C - c_p}{C - c_v}. \tag{1.21}$$

Comparing eqs. (1.13) and (1.21), we immediately get

$$\alpha = \frac{C - c_p}{C - c_v}. \tag{1.22}$$

For a perfect monoatomic gas c_p and c_v are both constants. You may recall from statistical thermodynamics that both c_p and c_v are related to the total number of degrees of freedom available to a gas "particle" in its interaction to neighbouring gas particles. The quantity C, on the other hand, is defined in terms of the (macroscopic) thermodynamic behavior of the system. What are the bounds on C ? One bound is the so-called *adiabatic* limit, i.e., no local heat input or drain ($\mathrm{d}Q = 0$); the only way to accomodate changes in temperature without violating eq. (1.18) is to have in this case $C = 0$. The other bound is the *isothermal* limit. By definition, isothermality implies that even a heat flow whose magnitude tends to infinity cannot locally affect the temperature; in view of eq. (1.18), this is only possible in the limit $C \to \infty$. Consequently, we have $0 \leq C < \infty$. From eq. (1.22), the corresponding bounds on α are

$$1 \leq \alpha \leq c_p/c_v. \tag{1.23}$$

The ratio of specific heat, c_p/c_v, is commonly denoted γ. You may recall that for a perfect monoatomic gas, $\gamma = 5/3$ in the non-relativistic limit. The range of acceptable values of α is quite narrow !

Running rapidly once again through the preceeding derivation, one should realize that up to this points all we have done is manipulate thermodynamic relations, without really making any simplifying assumptions beyond the perfect monoatomic gas hypothesis. Eq. (1.12), which was initially introduced as an assumption, is actually valid for any perfect gas with constant mean molecular weight. The actual *value* of α is a function of the local heat input/drain, which in general may be a function of space and/or time but is always constrained by eq. (1.23). So it seems that we have accomplished nothing. We eliminated the pressure $p(\mathbf{x}, t)$ via eq. (1.14)... at the cost of introducing a quantity $\alpha(\mathbf{x}, t)$. But this is where we introduce the *polytropic approximation*, which consists in assuming that the value of α is constant in space and/or time, and in most instances that this constant value can be specified *a priori* (or, alternately, treated as an adjustable parameter in a given model). It should be clear from the above discussion that this, implicitly, corresponds to enforcing a specific functional form for the heat input/drain dQ everywhere in the domain of interest. This is something we would normally get out of the energy equation. In that sense, the polytropic approximation can be seen as an alternative to actually *solving* the energy equation. Something like was to be expected, since within the framework of the polytropic assumption the pressure field is fully determined from the density profile (cf. eq. [1.14]). Adopting a relation such as eq. (1.14) while retaining the full set of hydrodynamical equations would overspecify the problem (One more equation than the number of unknowns !).

In forthcoming chapters, we sometimes be convenient to rewrite eq. (1.14) by directly defining the *polytropic sound speed* c_s^2 to be $\alpha p/\rho$, so that

$$\alpha p = c_s^2 \rho \qquad (1.24),$$

or, alternately

$$c_s^2 = c_{s0}^2 \left(\frac{\rho}{\rho_0}\right)^{\alpha-1}, \qquad (1.25)$$

with $c_{s0}^2 = \alpha p_0/\rho_0$. In the isothermal limit, eq. (1.14) can be written in the simpler form

$$p = a^2 \rho, \qquad (1.26)$$

where $a = \sqrt{kT/\mu m}$ is the *isothermal sound speed*, a constant in this case.

Consider what we have done. We are now in a position to express the ∇p term in the momentum equation in terms of ρ only (as opposed to ρ and T). From eqs. (1.24) and (1.25) one obtains immediately

$$\frac{1}{\rho}\nabla p = \frac{\alpha p_0}{\rho_0}\left(\frac{\rho}{\rho_0}\right)^{\alpha-1} \nabla\left[\ln\left(\frac{\rho}{\rho_0}\right)\right] = c_s^2 \nabla\left[\ln\left(\frac{\rho}{\rho_0}\right)\right], \qquad (1.27)$$

while in the isothermal case one obtains

$$\frac{1}{\rho}\nabla p = a^2 \nabla(\ln \rho). \qquad (1.28).$$

Notice how, in both cases, we have essentially eliminated two equations; the energy equation, which is what we were out to do in the first place, as well as the equation of state. This is because p no longer couples into the momentum equations, and can be computed directly from the density profile. In both cases, we now have to solve eqs. (1.1), (1.2), and (1.4), for the field variables $\mathbf{v}$, $\mathbf{B}$, and ρ, after which p and T can be obtained directly. With a few additional simplifying assumptions concerning the *geometry* of the problem, we now have a tractable problem.

1.4 An application: Static corona models

The solar corona being visible with the naked eye at times of total eclipses, we can assume that it was first observed a few million years ago by some hairy neanderthal with smelly armpits. However, it is only in the late 1930's that the solar corona was unambiguously recognized as being composed of very hot (1—2×10^6 K) ionized gas. The key in reaching that conclusion was the realization that many of the unidentified lines seen in coronal spectra were not unknown chemical elements, but instead belonged to high ionization stages of previously known elements (such as Calcium and Iron).

Since it is an observational fact that there *is* a hot corona out there, our task is now to construct a model allowing us to interpret these observations in a quantitative and coherent way; observations without models are a mere collection of unrelated facts. And models that make no testable predictions are hardly better than astrology. But enough philosophy, and lets dive into the mud.

We start with a simple model, which is usually a good idea. This model is simple because we construct it under the following assumptions: our model will represent a corona that is static ($\mathbf{v}=0$), in a steady-state ($\partial/\partial t=0$), spherically symmetric ($\partial/\partial\theta=0$, $\partial/\partial\phi=0$, $\partial/\partial r\to \mathrm{d}/\mathrm{d}r$), and unmagnetized ($\mathbf{B}=0$). We construct a solution above a reference radius r_0, at which the density (ρ_0) and temperature (T_0) are assumed known. We also assume that the corona is composed only of fully ionized hydrogen ($m=m_p=1.67\times10^{-24}$ gm, $\mu=0.5$).

The r-component of the equations of motion becomes a statement of hydrostatic balance:

$$\frac{\mathrm{d}p}{\mathrm{d}r}=-\rho\frac{GM_\odot}{r^2}, \tag{1.29}$$

where we have assumed a spherically symmetric gravitational potential $V=-GM_\odot/r$. This says nothing more that the (outward-directed) pressure gradient balances exactly the (inward-directed) gravitational acceleration, a particularly simple form of force balance. Using the equation of state $p=\rho\, kT/\mu\, m$, this can be rewritten as

$$\frac{\mathrm{d}\rho}{\rho}+\frac{\mathrm{d}T}{T}=-\frac{GM_\odot\mu m}{r^2kT(r)}\mathrm{d}r, \tag{1.30}$$

so that

$$\rho(r)=\rho_0\,\exp\left[-\frac{GM_\odot\mu\, m}{k}\int_{r_0}^{r}\frac{\mathrm{d}r}{r^2T(r)}-\int_{r_0}^{r}\frac{\mathrm{d}T}{\mathrm{d}r}\mathrm{d}r\right]. \tag{1.31}$$

To proceed further we must obtain an expression for the temperature profile in the corona. The simplest possibility is to assume that the corona is *isothermal*, i.e., $T(r)=T_0$. This leads immediately to

$$\frac{\rho(r)}{\rho_0}=\exp\left[-\frac{GM_\odot\mu\, m}{r_0kT_0}\left(1-\frac{r_0}{r}\right)\right], \tag{1.32}$$

with the pressure profile given by a similar expression:

$$\frac{p(r)}{p_0} = \exp\left[-\frac{GM_\odot \mu m}{r_0 k T_0}\left(1 - \frac{r_0}{r}\right)\right], \tag{1.33}$$

Clearly, neither the pressure nor density vanish at infinity for finite T_0. This should not really surprise us, since, by the isothermality assumption, the temperature remains constant as $r \to \infty$.

A more realistic corona can be constructed by assuming that a polytropic relationship exists between the pressure and density:

$$\frac{p}{p_0} = \left(\frac{\rho}{\rho_0}\right)^\alpha, \qquad 1 \leq \alpha \leq 5/3 \tag{1.34}$$

Using for conciseness the definition of the base polytropic sound speed $c_{s0}^2 = \alpha k T_0/\mu m$, the statement of hydrostatic balance (1.29) now becomes

$$c_{s0}^2 \left(\frac{\rho}{\rho_0}\right)^{\alpha-1} \mathrm{d}\rho = -\rho \frac{\mathrm{GM}_\odot}{\mathrm{r}^2} \mathrm{dr}, \tag{1.35}$$

which is readily integrated to yield an expression for the density profile

$$\frac{\rho(r)}{\rho_0} = \left[1 - \frac{(\alpha-1)GM_\odot}{r_0 c_{s0}^2}\left(1 - \frac{r_0}{r}\right)\right]^{1/(\alpha-1)}, \tag{1.36}$$

from which the pressure profile is immediately obtained via eq. (1.34):

$$\frac{p(r)}{p_0} = \left[1 - \frac{(\alpha-1)GM_\odot}{r_0 c_{s0}^2}\left(1 - \frac{r_0}{r}\right)\right]^{\alpha/(\alpha-1)}, \tag{1.37}$$

and the temperature profile from the equation of state:

$$\frac{T(r)}{T_0} = \left[1 - \frac{(\alpha-1)GM_\odot}{r_0 c_{s0}^2}\left(1 - \frac{r_0}{r}\right)\right]. \tag{1.38}$$

The first two of these expression are the polytropic equivalents of eqs. (1.32) and (1.33). The density, pressure and temperature profiles now depend on two parameters; the base temperature T_0 and polytropic index α. Unlike the isothermal case, it looks like there may be choices of T_0 and/or α that may yield zero pressure and density at a *finite* value of r. It is easily shown that this occurs whenever

$$c_{s0}^2 < \frac{(\alpha-1)GM_\odot}{r_0} \qquad r > r_0, \tag{1.39}$$

with

$$\frac{r_{\rm top}}{r_0} = \left(1 - \frac{r_0 c_{s0}^2}{(\alpha - 1)GM_\odot}\right)^{-1} \tag{1.40}$$

being the maximum radial extent of the polytropic atmosphere[7]. Eqs. (1.36) through (1.38) describe a static polytropic atmosphere occupying the volume $r_0 \leq r \leq r_{\rm top}$. For $r > r_{\rm top}$ there is only mathematical vacuum, something Nature abhors, or so Aristotle used to claim. What if T_0 is too large for eq. (1.39) to be satisfied ? Figure 1.1 illustrates a series of polytropic solar coronal models, for $T_0 = 1.5 \times 10^6\,{\rm K}$, $r_0 = 1.15\,R_\odot$, fully ionized hydrogen, and various values of α (for this adopted value of T_0 and for solar parameters, satisfying eq. (1.39) requires $\alpha > 1.1765$). It looks like the solutions that violate eq. (1.39) extend to infinity with non-vanishing pressures and densities. What is happening, physically, with these solutions ?

Could it be that these simply are not gravitationally bound given the adopted base temperature ? The criteria for gravitationally binding an atmosphere is not at all a simple one, but for the sake of the argument let's say that the average thermal energy of a particle should be significantly less than its gravitational binding energy:

$$kT_0 = f\frac{2GM_\odot \mu m}{r_0}, \tag{1.41}$$

where $f < 1$. If this criterion is not satisfied the atmosphere evaporates away. In terms of the polytropic sound speed,

$$c_{s0}^2 > (\alpha f)\frac{GM_\odot}{r_0}, \tag{1.42}$$

which is a different criterion from eq. (1.39). There exists a T_0 range given by

$$\left(\frac{\alpha - 1}{\alpha}\right)\frac{GM_\odot \mu m}{r_0 k} < T_0 < f\frac{GM_\odot \mu m}{r_0 k} \tag{1.43}$$

where our coronal models are gravitationally bound according to eq. (1.42), yet extends to infinity with non-vanishing pressures and densities... This is a T_0 range we call... the Twilight Zone... For $r_0 = 1.15\,R_\odot$ and $\alpha = 1.1$—1.2 for the Sun (based on spectroscopically deduced temperature profile in the corona), $10^6 \lesssim T_0 \lesssim 10^7\,{\rm K}$ (for $f = 1$, admittedly an extreme case). With $T_0 = 1.5$—$2 \times 10^6\,{\rm K}$ the solar corona is within this range. Of course it had to be...

---

[7] Prior to the advent of computers, polytropic gas spheres of finite radial dimension were extensively used to construct stellar/solar models. By superposing polytropes of various polytropic indexes, one can do a surprisingly good job at reproducing the runs of density, pressure, etc. with radius. Check out Chandrasekhar's 1939 textbook on stellar structure if you want to see how this was done.

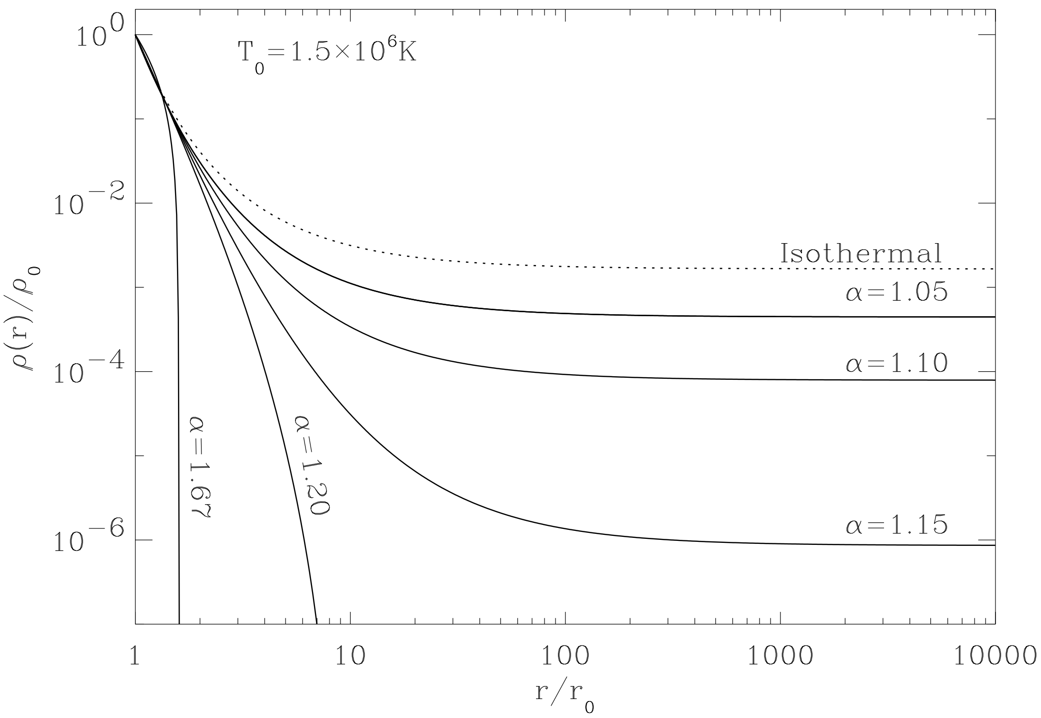

Figure 1.1: Density profiles for a few polytropic static coronal model with $T_0 = 1.5 \times 10^6\,$K. and $r_0 = 1,15\,R_\odot$. Note the asymptotically constant densities as $r \to \infty$ for $\alpha < 1.1765$.

Let's investigate the asymptotic (i.e. $r \to \infty$) behavior of our solutions at large distances in a bit more detail. From eqs. (1.36) through (1.38) one immediately obtains

$$\lim_{r\to\infty} \frac{\rho}{\rho_0} = \left[1 - \frac{(\alpha-1)GM_\odot}{r_0 c_{s0}^2}\right]^{1/(\alpha-1)}, \tag{1.44}$$

$$\lim_{r\to\infty} \frac{p}{p_0} = \left[1 - \frac{(\alpha-1)GM_\odot}{r_0 c_{s0}^2}\right]^{\alpha/(\alpha-1)}, \tag{1.45}$$

$$\lim_{r\to\infty} \frac{T}{T_0} = \left[1 - \frac{(\alpha-1)GM_\odot}{r_0 c_{s0}^2}\right], \qquad (1.46),$$

none of which generally vanishes, but we knew this already from Fig. 1.1. But what are the numerical values the RHSs? After all, there is not really a $T = 0$ perfect vacuum out there, there is the interstellar medium which, however tenuous, must be reckoned with. Again for $r_0 = 1.15\,R_\odot$, $T_0 = 1.5 \times 10^6\,$K, $\alpha = 1.1$, and $N_0 = \rho_0/(\mu m) = 10^8\,\mathrm{cm}^{-3}$, one obtains

$$\lim_{r\to\infty} \left(\frac{\rho}{\mu m}\right) = 10^4\,\mathrm{cm}^{-3}, \tag{1.47}$$

$$\lim_{r\to\infty} p = 8 \times 10^{-7}\,\text{dyne cm}^{-2}, \tag{1.48}$$

$$\lim_{r\to\infty} T = 6 \times 10^{5}\,\text{K}. \tag{1.49}$$

These values are much larger than anything the interstellar medium has to offer. In the solar galactic neighborhood, typical densities and temperatures are believed to be $N_{\rm ISM} = 1\,{\rm cm}^{-3}$ and $T_{\rm ISM} = 100$ K, so that $p \sim 10^{-14}$ dyne cm^{-2}. All of these are insufficient by orders of magnitude[8]. Something is deeply wrong. Given the assumptions made in constructing our simplistic model, two avenues are open to "save" our model:

(1) Abandon the hypothesis of a steady-state ($\partial/\partial t = 0$) corona,

(2) Work on the energetics to produce a corona with a different asymptotic temperature profile,

(3) Abandon the hypothesis of a static ($\mathbf{v} = 0$) corona.

Possibility (1) flies in the face of observations, at least as far as the larger spatial scales are concerned. Early efforts (and efforts to come; see problems 1.1 and 1.2 !) were mostly directed along avenue (2). Yet avenue (3) proved to be the right one. This is the topic of the next chapter.

Problems

(1.1) The purpose of this problem is to get you to construct a coronal model that is more realistic, energetically speaking, than the isothermal and polytropic models discussed in this chapter. Your starting point is the assumption that *thermal conduction* dominates the energy transport in the corona. For a static and steady-state corona, the energy equation then reduces to

$$\nabla \cdot (\chi \nabla T) = 0.$$

where χ is the coefficient of thermal conductivity. In a low density, high temperature plasma of fully ionized hydrogen, an approximate (yet fairly accurate) expression for κ is

$$\chi(T) = \chi_0 T^{5/2},$$

where $\chi_0 \simeq 8 \times 10^{-7}$ erg cm^{-1} s^{-1} K$^{-7/2}$. So your task is the following:

---

[8] Actually, a realistic estimate of the *total* pressure in the interstellar medium should take into consideration the contribution of the interstellar magnetic field. Far from being negligible, magnetic pressure can provide $\sim 10^{-12}$ dyne cm^{-2} for $||\mathbf{B}||_{\rm ISM} \sim 10^{-5}$ G. But this is still insufficient to equilibrate our hot hydrostatic corona.

(a) Obtain expressions for $T(r)$, $\rho(r)$, and $p(r)$, and plot these as a function of r for a few values of T_0 in the range $10^6 \leq T_0 \leq 5 \times 10^6$ K.
(b) Obtain asymptotic ($r \to \infty$) expression for $T(r)$, $\rho(r)$ and $p(r)$, and calculate these asymptotic values for the solutions you obtained in (a)
(c) Compare and contrast your results in (b) with the corresponding results for the polytropic coronae discussed at the end of this chapter.
(d) What is the energy input (erg s^{-1}) require to maintain the corona in its assumed steady state, given the outward transport of energy ? Can you think of other important coronal energy "sinks" ?

(1.2) This problem further explores possible "fixes" for our static coronal models.

(a) Determine how fast the temperature profile would have to fall with distance for the pressure to vanish at infinity in a static corona.
(b) what should be the coronal temperature for a static, *isothermal* corona to by dynamically balanced by the pressure in the interstellar medium?

Bibliography

Among the numerous good books available on classical fluid mechanics, the following are noteworthy:

Batchelor, G.K. 1967, *An introduction to Fluid Dynamics* (Cambridge: Cambridge University Press)
Landau, L.D., & Lifshitz, E.M. 1959, *Fluid Mechanics* (Oxford: Pergamon Press)

Derivations of the induction equation (2.11) from the Maxwell equations in the MHD limit can be found in a number of places, be it books on electrodynamics or specifically on astrophysical magnetohydrodynamics. For example:

Jackson, J.D., *Classical Electrodynamics* (New York: John Wiley), chap. 10 (second edition)
Parker, E.N. 1979, *Cosmical Magnetic Fields* (Oxford: Clarendon Press), chap. 4.
Shu, F.H. 1992, *The Physics of Astrophysics. Vol. II: Gas Dynamics* (Mill Valley: University Science Books), chap. 21.

Shu's book also contains an accessible discussion of the passage from (discrete) kinetic theory to the (continuous) fluid limit (chap. 2). More technical but also recommended in that context are

Braginskii, S.I. 1965, *Rev. Plasma Phys.*, **1**, 205.
Cannon, C.J. 1985, *The Transfer of Spectral Line Radiation* (Cambridge: Cambridge University Press), chap. 5.

The first reasonably realistic models for hydrostatic coronae were constructed by

Chapman, S. 1957, Smithsonian Contrib. Ap., 2, 1.

Evidence for the existence of ionized gas (static or not) in the interplanetary environment was first infered on the basis of the measured polarization of zodiacal light. The classic reference is

Behr, A., & Siedentopf, H. 1953, Z. Ap., 32, 19.

Empirical modelling of the corona, based on observational material, can also be carried out to yield insight into its large-scale structure. For different lines of attack on this problem see, e.g.,

Withbroe, G.L. 1988, ApJ, 325, 442.
Bagenal, F., & Gibson, S. 1991, JGR, 96, 17663

2. THERMALLY-DRIVEN WINDS: I. ISOTHERMAL MODEL

A fool sees not the same tree that a wise man sees
No bird soars too high if he soars with his own wings
If the fool would persist in his folly he would become wise
What is now proved was once only imagin'd

William Blake
The Marriage of Heaven and Hell (1793)

In this section we will construct the simplest, yet reasonably realistic, solar wind model. A thorough understanding of this simple model is essential, both for getting a good grasp of the relevant physics and for being able to interpret the more detailed solar wind models to be constructed in the upcoming sections. But this model also does a surprisingly good job at reproducing a lot of the large-scale flow properties of the real solar wind.

2.1 A flow example: the de Laval nozzle

It is instructive to first consider an even simpler example, in cartesian geometry. Consider a *nozzle*, i.e., an axially symmetric tube, oriented parallel to the x-axis, with a cross-section σ which is a function of x (see Fig. 2.1). Suppose now that an *incompressible* fluid ($\rho =$const.) is forced to flow in the nozzle. In a steady-state ($\partial/\partial t = 0$), the mass conservation equation can be integrated directly to yield the constraint $\sigma v_x =$ const., i.e., the flow velocity varies in inverse proportion to the cross-section of the nozzle. For a converging tube ($\partial\sigma/\partial x < 0$), the flow accelerates, while for a diverging tube the flow decelerates. So far so good, no surprises.

Consider now a similar nozzle, in which this time a *compressible* fluid is forced to flow. The mass conservation equations yields the constraint

$$\sigma\rho v_x = \text{const.} \tag{2.1}$$

In cartesian geometry, neglecting gravity, and in a steady-state, the only relevant component of the equations of motions is the x-component, which reduces to

$$v_x \frac{\partial v_x}{\partial x} = -\frac{1}{\rho}\frac{\partial p}{\partial x}. \tag{2.2}$$

Figure 2.1: Schematic representation of a nozzle. The flow has a component only in the x-direction, i.e., along the axis of the nozzle. The latter has a varying cross-section σ which is some yet undetermined function of x.

If the flow is adiabatic (see §1.3), the RHS of this expression can be manipulated into

$$\frac{1}{\rho}\frac{\partial p}{\partial x} = c_s^2 \frac{\partial}{\partial x}\left[\ln\left(\frac{\rho}{\rho_0}\right)\right] = -c_s^2\left[\frac{1}{\sigma}\frac{\partial \sigma}{\partial x} + \frac{1}{v_x}\frac{\partial v_x}{\partial x}\right] \qquad (2.3),$$

which allows eq. (2.2) to be rewritten as

$$\frac{1}{v_x}\left[\left(\frac{v_x}{c_s}\right)^2 - 1\right]\frac{\partial v_x}{\partial x} = \frac{1}{\sigma}\frac{\partial \sigma}{\partial x}. \qquad (2.4)$$

What does this tell us about the behavior of the flow? Consider then the following sets of situations:

- The flow is subsonic ($v_x < c_s$)
  - (i) Converging tube ($\mathrm{d}\sigma < 0$): Eq. (2.4) yields $\partial v_x/\partial x > 0$, i.e., the flow accelerates.
  - (ii) Straight tube ($\mathrm{d}\sigma = 0$): Eq. (2.4) yields $\partial v_x/\partial x = 0$, i.e., uniform flow speed.
  - (iii) Diverging tube ($\mathrm{d}\sigma > 0$): Eq. (2.4) yields $\partial v_x/\partial x < 0$, i.e., the flow decelerates.
- The flow is supersonic ($v_x > c_s$)
  - (i) Converging tube ($\mathrm{d}\sigma < 0$): Eq. (2.4) yields $\partial v_x/\partial x < 0$, i.e., the flow decelerates.
  - (ii) Straight tube ($\mathrm{d}\sigma = 0$): Eq. (2.4) yields $\partial v_x/\partial x = 0$, i.e., uniform flow speed.

(iii) Diverging tube ($d\sigma > 0$): Eq. (2.4) yields $\partial v_x/\partial x > 0$, i.e., the flow accelerates[1].

In the subsonic case, the behavior of the flow is qualitatively similar to that of an incompressible flow. But for a supersonic flow, the behavior is totally different[2], indicating that proper handling of compressibility is essential to transonic/supersonic flow computations[3]

2.2 Thermally-driven winds: the isothermal solution of Parker

The simple nozzle problem studied demonstrates that under certain conditions it is possible to "spontaneously" convert the thermal energy of a gas globally at rest into large-scale flow kinetic energy. Is this something that can happen only in nozzles ? The answer is no. It works with stars also, but again only under certain conditions.

We will now attempt to construct a simple model for a thermally-driven wind emitted by a non-rotating, non-magnetic star. We will follow here the initial approach of E.N. Parker, in seeking steady state ($\partial/\partial t = 0$) solutions that are spherically symmetric ($\partial/\partial\theta = 0$, $\partial/\partial\phi = 0$). This also implies $v_\theta = 0$, $v_\phi = 0$ (think about it a bit). We *assume* that the star is surrounded by a hot corona (temperature T_0 of the order of 10^6 K), as in §1.4 extending outward from a reference radius $r = r_0$ where the base temperature and density are known. We seek a wind solution in the domain $r \in [r_0, \infty]$. We consider an inviscid ($\tau = 0$), unmagnetized ($\mathbf{B} = 0$) plasma. We will also limit ourselves to a *single fluid* model. That is, we consider a wind composed exclusively of fully ionized Hydrogen where charge neutrality always holds down to the smallest spatial scales considered[4]. This implies that the proton-electron mixture can be treated as a single fluid, with each particle having a mass $\mu\, m$, with $\mu = 0.5$.

In view of the spherical symmetry assumption, the mass conservation equation reduces to

$$\frac{1}{r^2}\frac{\partial}{\partial r}(r^2 \rho v_r) = 0. \tag{2.5}$$

which integrates directly to

$$\rho r^2 v_r = \text{const.} \tag{2.6}$$

[1] How far beyond the speed of sound do you think a diverging nozzle can accelerate a flow which, initially, is only mildly supersonic? For adiabatic flow such as the one considered here, the answer is $\sqrt{3}c_s$, *independently of the shape $\sigma(x)$ of the nozzle.* Can you figure that one out?

[2] How does automotive traffic behave, like an incompressible flow, or a supersonic compressible flow ? Think what happens when a lane is closed for construction on the interstate...

[3] How would you design a nozzle in such a way as to accelerate an initially subsonic flow to supersonic velocities?

[4] Does that also mean that protons and electrons must have identical bulk velocities? Think about that one a bit.

We only have to deal with the r-component of the equations of motion:

$$\rho v_r \frac{\partial v_r}{\partial r} = -\rho \frac{GM_\odot}{r^2} - \frac{\partial p}{\partial r} \tag{2.7}$$

where we have again assumed a spherically symmetric gravitational potential $-V = GM_\odot/r$. For simplicity, we will focus on *isothermal* solutions. You will recall from §1.3 that this corresponds to replacing the energy equation (1.3) by the statement $T(r) = T_0$, and that the equation of state then becomes

$$p = a^2 \rho, \tag{2.8}$$

where $a = \sqrt{kT/\mu m}$ is the isothermal sound speed. Using (2.8), and then (2.6), eq. (2.7) becomes

$$\begin{aligned} v_r \frac{\partial v_r}{\partial r} &= -\frac{GM_\odot}{r^2} - \frac{a^2}{\rho}\frac{\partial \rho}{\partial r} \\ &= -\frac{GM_\odot}{r^2} + a^2\left(\frac{1}{v_r}\frac{\partial v_r}{\partial r} + \frac{2}{r}\right), \end{aligned} \tag{2.9}$$

which can be manipulated into

$$\frac{\partial v_r}{\partial r} = \frac{v_r}{r}\left(\frac{2a^2 - GM_\odot/r}{v_r^2 - a^2}\right). \tag{2.10}$$

This is a *non-linear* ODE. Therefore, we can expect that it will accept many families of solutions in the form $v_r(r)$. There is a lot to be learned from this differential equation, even before solving it! Note that the RHS diverges if the flow is transonic ($v_r^2 = a^2$ at some r). Unless of course the numerator on the RHS also goes to zero as $v_r \to a$. This can only occur at a radius

$$r_s = \frac{GM_\odot}{2a^2} \tag{2.11}$$

called the *sonic point*[5] ("sonic sphere" would actually be more appropriate in this case). In the language of mathematics, (r_s, a) is a *critical point* of the ODE (2.10).

We have already learned something important about the solution we are seeking, but we still have not solved the ODE, i.e., obtained the v_r vs r functional dependence. Lets return to solving the differential equation (2.7). With some manipulations, it can be recast in the form

$$\frac{\partial}{\partial r}\left[\frac{v_r^2}{2} + a^2 \ln\left(\frac{\rho}{\rho_0}\right) - \frac{GM_\odot}{r}\right] = 0, \tag{2.12}$$

[5] Does this mean that there can only be one and only one transonic solution? Look again at eq. (2.10) and think about it.

This integrates to

$$\frac{v_r^2}{2} + a^2 \ln\left(\frac{\rho}{\rho_0}\right) - \frac{GM_\odot}{r} = E \qquad (2.13),$$

where E is a constant[6]. We can express ρ as a function of r and v_r using eq. (2.6), so that solutions of eq. (2.10) are *all* the $v_r(r)$ curves satisfying

$$E(r, v_r) = \text{const.} \qquad (2.14)$$

So solving non-linear ODEs is easy? Not so fast; there are an *infinity* of acceptable solutions. How do we pick the right one[7]?

Figure 2.2 illustrates the various families of solutions of the form $E(r, v_r)$ =const. There are *two* transonic solutions, indicated by thicker lines. They meet at the sonic point, and divide the $[v_r, r]$ plane into four regions (very originally labeled I through IV). Solutions in regions II and IV are unphysical, in that v_r is not a single-valued function of r. More intuitively, they are not wind solutions since they do not "connect" $r = r_0$ to $r \to \infty$. Solutions in region I are always supersonic, and in region III always subsonic. Observations clearly rule out solutions that are supersonic at the base of the corona. This leaves us with either class III solutions, or the one transonic solutions with $\partial v_r/\partial r > 0$. The latter does not differ much from class III solutions near the reference radius r_0, but does differ drastically beyond the sonic point; class III solutions deccelerate rapidly beyond r_s, while the transonic solution more or less levels off at supersonic velocities beyond a few r_s. Spacecraft measurements clearly show that the solar wind is supersonic in the vicinity of 1 AU, thus ruling out class III solutions and leaving us with a single transonic solution. [8] [9].

There is something nice about this (isothermal) transonic solution. It is *uniquely* specified once a given value of T_0 is adopted (with r_0 and $M_\odot$ also given, of course)[10]. Figure 2.3 illustrate a number of such transonic solutions, computing using various values for the base temperature T_0, while keeping r_0 fixed. Note the following:

---

[6] To what does this constant correspond? Examine carefully the terms on the LHS of eq. (2.13) and figure it out.

[7] The answer is *not* "by evaluating E at the base of the corona". Go back to eq. (2.13), and you will realize that evaluating E at r_0 requires *also* the knowledge of v_r at r_0. And this *cannot* be specified *a priori*. Do you know why?

[8] Try "designing" an nozzle (i.e., compute a $\sigma(x)$ function) that would yield the same isothermal flow profile than found here for the isothermal solar wind.

[9] It turns out that class III solutions are also unphysical, but for somewhat subtler reasons having to do with the asymptotic behavior of the solutions at large radial distances. This issue is explored further... in problem 2.3 !

[10] What happens in the limit $T_0 \to 0$? One should expect that in the absence of a corona, no thermally driven wind solution should exists Is this the case here? How do you explain this? After all —and fortunately—, the Earth's atmosphere does not seem to be expanding supersonically... or does it ?

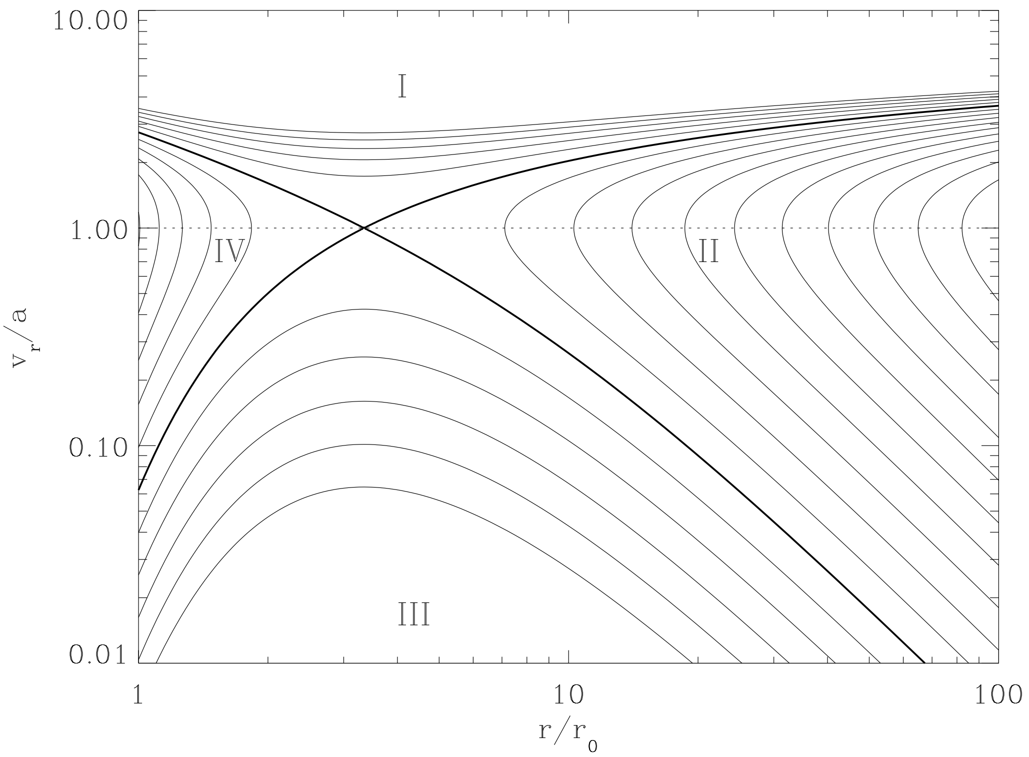

Figure 2.2: Topology of the isothermal solution of Parker, for a thermally-driven wind. Each curve is a E =constant locus, and represents an acceptable solution, from the standpoint of global energy conservation. Yet a number of these curves are dynamically unphysical. The dotted line is the sound speed, independent of r in the isothermal case.

- As T_0 is increased, the sonic point moves closer to the reference radius[11].
- As T_0 is increased, the asymptotic flow speed ($r \to \infty$) increases, and does so faster than the sound speed
- In all cases, most of the wind's acceleration occurs in the subsonic ($r < r_s$) region.

Lets now try to obtain a full solution, i.e., a relationship for $v_r(r)$ vs r. Our first step in doing so is to obtain an expression for the wind speed at the reference radius. Evaluate first E at the sonic point. Making use of (2.6) and (2.11), one

[11] In particular, note that on Fig. 2.3 the 5×10^6 K solution has its critical point located *below* the reference radius. You can verify that the temperature at which this occurs is $T_{0c} = GM_\odot \mu m / 2kr_0$, which for the Sun is $T_c \simeq 4 \times 10^6$ K. The critical point actually sits under the Sun's surface ($R_\odot \simeq 6.96 \times 10^{10}$ cm) for $T_{0s} \simeq 5.8 \times 10^6$ K. Does this mean that no transonic wind is possible from a corona hotter than these critical temperatures?

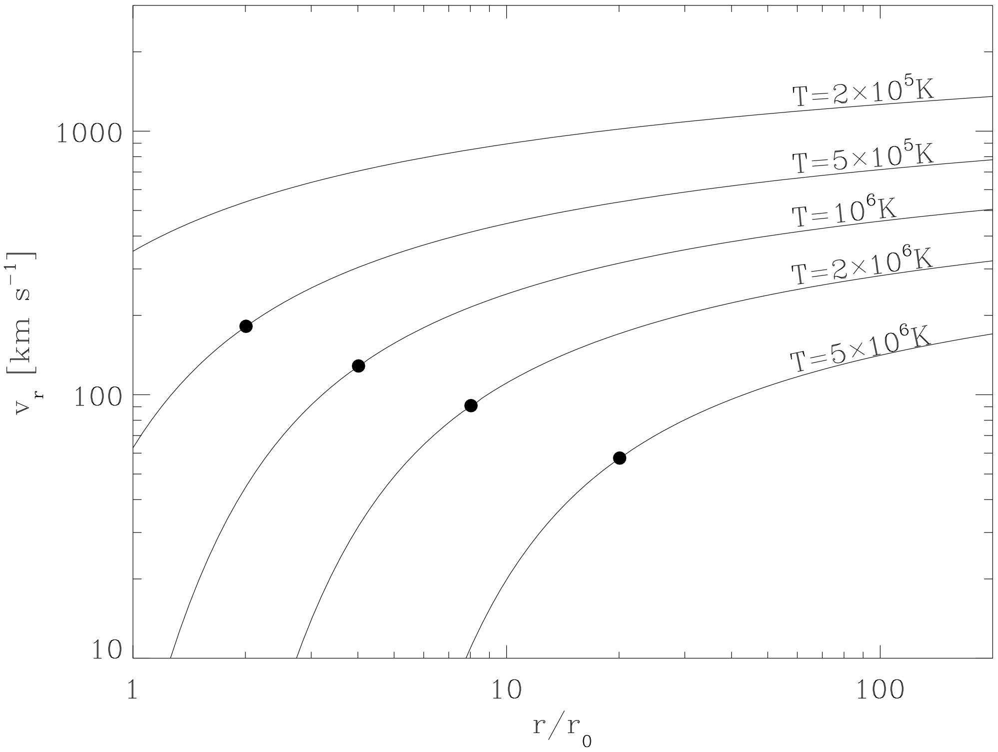

Figure 2.3: Sequence of Parker-type transonic solutions for thermally-driven winds, for various coronal base temperature. The solid dots indicate the position of the sonic point for each solution. The earth's orbit is also indicated.

obtains

$$\frac{E_s(r_s,a)}{a^2} = -\frac{3}{2} + \ln\left[\frac{v_{r0}}{a}\left(\frac{r_0}{r_s}\right)^2\right], \tag{2.15}$$

where v_{r0} is the radial velocity evaluated at the reference radius r_0. Evaluate now E at the reference radius:

$$\frac{E_0(r_0,v_{r0})}{a^2} = \frac{1}{2}\left(\frac{v_{r0}}{a}\right)^2 - 2\left(\frac{r_s}{r_0}\right). \tag{2.16}$$

Recall that we are studying transonic solutions, i.e., solutions that are very subsonic at $r = r_0$, and for which $r_s/r_0 \sim 2$—10. This means that on the RHS of eq. (2.16), the second term is much larger than the first. We can then approximate E_0 by

$$\frac{E_0(r_0,v_{r0})}{a^2} \simeq -2\left(\frac{r_s}{r_0}\right). \tag{2.17}$$

Equating eqs. (2.15) and (2.17), one obtains after some manipulation

$$\frac{v_{r0}}{a} = \left(\frac{r_s}{r_0}\right)^2 \exp\left[\frac{3}{2} - 2\frac{r_s}{r_0}\right], \qquad v_{r0} \ll a. \tag{2.18}$$

Figure 2.4: Mass flux at earth's orbit, as a function of coronal base temperature. The base density is held constant at $N = 10^8$ cm^{-3}.

This allows us to compute an expression for the mass loss rate

$$\dot{\mathrm{M}} = 4\pi \rho_0 r_0^2 v_{r0}, \tag{2.19}$$

or, alternately, the mass flux (gm cm^2 s^{-1}) at a given distance r:

$$\Phi = 4\pi \rho_0 v_{r0} \left(\frac{r_0}{r}\right)^2 . \tag{2.20}$$

Figure 2.4 shows the variations of the mass flux at 1AU as a function of coronal base temperature, for a fixed value of base density[12]. Note how the mass flux increases rapidly with coronal base temperature. This is only in part due to the increase in wind speed at 1AU with increasing temperature (cf. Fig. 2.3), yet the bulk of the increase is due to the larger densities at 1 AU in the hotter models. This is not surprising; if more thermal energy is available, more mass can be lifted out of the Sun's gravitational potential.

---

[12] How about obtaining an approximate expression for the asymptotic (i.e., $r \to \infty$) wind velocity ($v_{r\infty}$, say). This should be feasible, especially since on Fig. 2.3 it looks like $v_r \to$ constant as $r \to \infty$. Computing E in the limit of large r and equating to E_s, we get

$$\left(\frac{v_{r\infty}}{a}\right)^2 = -3 + 2 \ln \left[\frac{v_{r\infty}}{a} \left(\frac{r}{r_s}\right)^2\right],$$

the RHS of which diverges logarithmically as $r \to \infty$! How can this be possible? Hint: the answer to this apparent paradox is related to the question posed in footnote #10

How about obtaining an expression for $v_r(r)$ valid at any r? Equating $E(r, v_r)$ to E_s yields, after some manipulations,

$$\frac{1}{2}\left(\frac{v_r}{a}\right)^2 - \ln\left[\left(\frac{r}{r_s}\right)^2\left(\frac{v_r}{a}\right)\right] = \left(\frac{3}{2} - 2\frac{r_s}{r}\right), \tag{2.21}$$

Do not lose sleep over trying to isolate v_r in this expression. Equation (2.21) is a *transcendental* equation in v_r, which has no closed form solution and can only be solved iteratively. To do this we rewrite is as

$$v_r = a\left\{4\left(\frac{r_s}{r}\right) - 3 + 2\ln\left[\left(\frac{r}{r_s}\right)^2\left(\frac{v_r}{a}\right)\right]\right\}^{1/2}, \tag{2.22}$$

the solution strategy is the following:

(1) Select a value of r and make a starting guess for $v_r^{(0)}$
(2) Using these, calculate the RHS of eq. (2.22) to obtain $v_r^{(1)}$. Not surprisingly, $v_r^{(1)} \neq v_r^{(0)}$ (unless we just happened to guess the right value for v_r. Unlikely).
(2) Use now $v_r^{(1)}$ on the RHS of eq. (2.22) to compute $v_r^{(2)}$. In all likelyhood, $v_r^{(2)}$ differs less from $v_r^{(1)}$ than $v_r^{(1)}$ differed from $v_r^{(0)}$.
(4) Keep iterating this way until $v_r^{(n)} \simeq v_r^{(n-1)}$ to within the desired accuracy.

Table 2.1 below illustrates the procedure in the case of the solution depicted on Fig. 2.2, for $r = 37.4\,r_s$ [13]. Convergence to 10^{-6} is in this case attained within 7 iterations[14]. Not bad. We will encounter this procedure again and again in the following pages, so you should really try it out for yourself[15]. For those with computer phobia, it works even with a pocket calculators. It just takes longer.

---

[13] Anything special about the value $37.4\,r_s$?

[14] Try repeating the procedure with $r = r_0$, in order to verify the accuracy of the approximate expression that we obtained previously for v_{r0} [eq. (2.18)]. What is happening (Hint: Go back to Figure 2.2 to try to understand this)? Can you modify the scheme in order to obtain the right solution?

[15] Those of you with a bit of experience in numerical matters will have already recognized that the method proposed here is a quick and dirty and somewhat peculiar way to solve the non-linear root finding problem for $v_r(r)$ defined by setting

$$E(r, v_r) - E_s(r_s, a) = 0$$

with r fixed. Any of the numerous methods available to solve such root finding problems can be used... with some care in the vicinity of the critical point ! More on this in the next chapter...

Table 2.1

Convergence of iterative scheme for eq. (2.22) with $r = 37.4\, r_s$

n	$v_r^{(n)}/a$	Δ	n	$v_r^{(n)}/a$	Δ
1	3.4042362	2.4042362	5	3.7742782	0.0000335
2	3.7468474	0.1006426	6	3.7742870	0.0000023
3	3.7723539	0.0068075	7	3.7742876	0.0000002
4	3.7741519	0.0004766			

Once $v_r(r)$ is known, the density profile $\rho(r)$ can be computed directly via eq. (2.6):

$$\rho(r) = \rho_0 \left(\frac{v_{r0}}{v_r}\right)\left(\frac{r_0}{r}\right)^2 , \tag{2.23}$$

and then the pressure profile via eq. (2.8):

$$p(r) = a^2 \rho(r). \tag{2.24}$$

Clearly, p vanishes as $r \to \infty$, in view of the $1/r^2$ dependence of the density profile and the fact that $v_r(r)$ is a monotonically increasing function of r [16].

A more intuitively appealling expression for $\rho(r)$ can be obtained by equating eq. (2.13) evaluated at the reference level r_0 and at radius r. Solving for ρ in the resulting expression yields

$$\rho(r) = \rho_0 \exp\left[-\frac{GM_\odot \mu m}{r_0 k T_0}\left(1 - \frac{r_0}{r}\right) - \frac{\mu m}{2kT_0}(v_r^2 - v_{r0}^2)\right]. \tag{2.25}$$

Compare this expression with eq. (1.36), obtained for a *static*, isothermal corona. Were it not for the presence of the second term in the exponential, these two

[16] At which distance do we have $p(r) \sim p_{\rm ISM}$? The question is actually not very meaningful, as eq. (2.24) gives the usual *gas* pressure at distance r, i.e., the isotropic pressure due to random thermal motions of the gas particles. In supersonic flows, the pressure is often dominated by the (non-isotropic) *ram pressure.* For our spherically symmetric flow, this is

$$p_{\rm RAM} \simeq \rho v_r^2 ,$$

and is directed radially outward. Using the fact that v_r is nearly constant for $r \gg r_s$, find the distance at which $p_{\rm RAM} \simeq p_{\rm ISM}$. How does this compare with the orbital radii of the outer planets? What does that tell you about the validity of our assumption of a freely expanding corona? Actually, how do you think a supersonic wind can "terminate" in the interstellar medium?

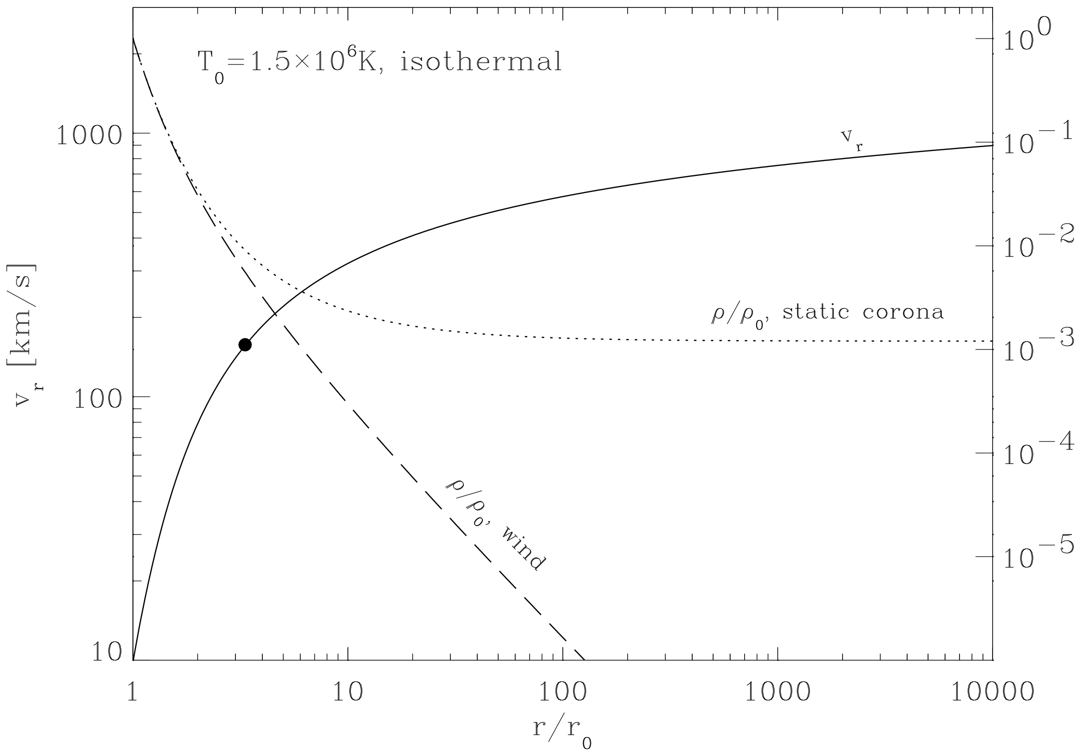

Figure 2.5: A full solution for $T_0 = 1.5 \times 10^6$ K and $r_0 = 1.15\, R_\odot$.

expressions would be *identical.* You can verify that the ratio of the second to first term increases with distance. Yet, at the sonic point, this ratio is only ~ 0.1. This means that below $r = r_s$, the structure of the expanding corona is very much like that of a static isothermal corona. Beyond r_s, the ratio increases rapidly, and the structure is markedly different from that of a static isothermal corona. This is illustrated on Fig. 2.5, showing a full isothermal wind solution for $T_0 = 1.5 \times 10^6$ K and $r_0 = 1.15\, R_\odot$. The dotted line shows the expected density profile for a static isothermal corona with the same base temperature[17].

2.3 Force balance in the Parker isothermal solution

We now turn to the issue of *force balance* in our isothermal wind solution. This is illustrated on Figure 2.6, for the same $T_0 = 1.5 \times 10^6$ K solution as on Fig. 2.5. Note how the thermal pressure acceleration exceeds, even if sometimes only slightly, the gravitational acceleration throught the flow [18] [19]. It had better be, otherwise we

[17] Why do you think I did not bother plotting the pressure profile $p(r)$ on Fig. 2.5?

[18] See the little "glitch" in the thermal acceleration at $r/r_0 \simeq 3.5$? Any idea where this may come from ?

[19] Can you sketch a similar plot for the force balance in the isothermal static

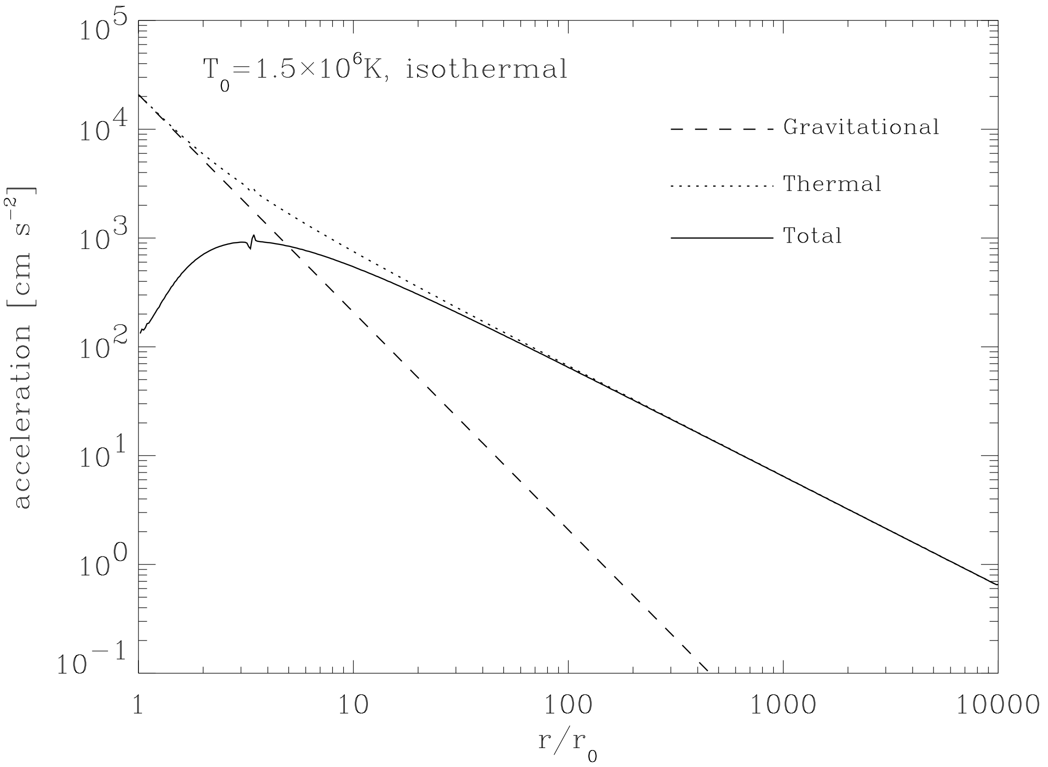

Figure 2.6: Contributions from to net wind acceleration (i.e., force per unit mass; Newton, remember...) in the Parker isothermal solution. Note how the thermal pressure largely exceeds the gravitational acceleration only at rather large distances; within the sonic point, gravity almost (but not quite) balances the thermal pressure gradient.

would have had a jolly hard time accelerating a wind to supersonic velocities. Note that at large distances the thermal acceleration decreases more slowly than gravity with distance ($\propto r^{-1}$, as opposed to r^{-2} for gravity). This, clearly, is the direction in which to look to explain the aforementioned logarithmic divergence of the flow velocity as $r \to \infty$... but that is for later.

2.4 Comparison with the "real" solar wind

We are now ready to compare our results to the "real" solar wind, as it is observed e.g. at the Earth's orbit[20]. Even though it had been realized earlier in this century

---

corona ?

[20] This is where, traditionally, most data has been coming from, although the space probes *Pioneer* and *Voyager* have provided (and are still providing!) data concerning the properties of the solar wind beyond the Earth's orbit, and as you are reading this the probe *Ulysses* is relaying to Earth solar wind data out of the ecliptic plane. So, Table 2.2 is just the beginning of the story.

that episodic mass outflows from the Sun were responsible for phenomena such as aurorae and geomagnetic storms. evidence for the presence of a *continuous* corpuscular outflow from the Sun was only put forth in the 1950's. This hinged on two apparently unrelated observational facts: (1) the strong polarization of zodiacal light, and (2) the large acceleration of comet tails. The first fact pointed out to the presence of free electrons, with density $N \sim 10^3\text{cm}^{-3}$, near the Earth, and the second to the existence of a radially directed (with respect to the Sun) ionized particle flux of order $10^{10}\text{cm}^{-2}\,\text{s}^{-1}$ at 1 AU. The *in situ* observation of this outflow, in the and early 60's, was a spectacular vindication of Parker's hypothesis.

The first difficulty one encounters in confronting models and observations is that the properties of the solar wind at the Earth's orbit are anything but constant, as exemplified by the amplitude of the fluctuations ($\pm$) in the first column of Table 2.2 below. These are real fluctuations, not error bars associated with the measurements themselves. Strangely enough, a sequence of measurements at successive times does not yield a gaussian-like distributions of measures. Instead it seems that the solar wind exists in two "modes", which have been dubbed *Low speed streams* and *High speed streams.* If the observational data is first subdivided into these two modes, relative fluctuations diminish drastically (see second and third columns in Table 2.2). Note in particular the remarkable constancy of the flow speeds. Traditional wisdom has been to associated high speed streams with open magnetic field regions of the corona, and low speed streams with closed magnetic field regions, but of course it is nowhere as simple as that...

Table 2.2

Properties of the solar wind at 1 AU

Parameter	Average	Low speed streams	High speed streams
N [cm^{-3}]	8.7±6.6 (76%)	11.9±4.5 (38%)	3.9±0.6 (15%)
v [$\text{km}\,\text{s}^{-1}$]	468±116 (25%)	327±15 (5%)	702±32 (5%)
Nv [$10^8\,\text{cm}^{-2}\,\text{s}^{-1}$]	3.8±2.4 (63%)	3.9±1.5 (38%)	2.7±0.4 (15%)
ϕ_v (degrees)	−0.6±2.6 (430%)	+1.6±1.5 (94%)	−1.3±0.4 (31%)
T_p (10^5 K)	1.2±0.9 (75%)	0.34±0.15 (44%)	2.3±0.3 (13%)
T_e (10^5 K)	1.4±0.4 (29%)	1.3±0.3 (20%)	1.0±0.1 (8%)
T_α (10^5 K)	5.8±5.0 (86%)	1.1±0.8 (68%)	14.2±3.0 (21%)

One also observes, superposed on both slow and high speed streams, transient events associated with the passage at the earth's orbit of MHD *shocks.* These can be traced to eruptions, flares, coronal mass ejections and the like, occurring in the lower corona. As these disturbances are advected outward by the solar wind, they steepen into shocks. It is the interaction of these disturbances with the

Earth's magnetosphere that is responsible for aurorae and geomagnetic storms[21]. We will not concern ourselves with such transient events here, but the book by Hundhausen, cited in the bibliography, discusses in some detail the formation and propagation of shocks in the solar wind.

Back to our model. Table 2.3 lists the radial velocities, densities and mass fluxes at selected radial positions of interest, for the isothermal wind solution of Fig. 2.4. Comparing the third line of this table to Table 2.2, one can only conclude that our simplistic wind model does a pretty decent job at predicting the average solar wind properties at 1 AU. Of course we are completely off on the temperature at 1 AU, but this should not come as a surprise in view of the isothermality assumption.

Table 2.3

Properties of Parker wind solution for $T_0 = 1.5 \times 10^6$ K and $N_0 = 10^8 \text{cm}^{-3}$

r	v_r [$\text{km}\,\text{s}^{-1}$]	N [cm^{-3}]	T [K]
r_0	9.8	10^8	1.5×10^6
r_s	158	5×10^5	1.5×10^6
$r_\oplus$	629	4	1.5×10^6
$10\, r_\oplus$	797	0.33	1.5×10^6

But let's not rejoice prematurely. Look at what is happening to the density. It falls rapidly with distance past the sonic point. Recalling the arguments made in §1.2, we can expect that at some point (1) our single fluid model will fail, and (2) our basic MHD formulation will become inadequate[21]. Our MHD or fluid equations were obtained, remember, by taking moments of the Boltzmann equation, itself resting on the assumption that a meaningful distribution in the 6-D $[\mathbf{x}, \mathbf{v}]$ phase space could be constructed. Now, the criteria for that, we argued heuristically, was that each cell in phase space should be populated with a reasonably large

[21] In particular, this was well known, if not quantitatively understood, by the beginning of Word War II. Since geomagnetic storms have an annoying tendency to perturb radio communications, it became of "strategic importance" to monitor the Sun continuously for the appearance of large flares or unusually high activity. This lead to the foundation of the High Altitude Observatory in the US, and of what became the Kiepenheuer Institut für Sonnenphysik in Germany. This is not to say that wars are useful things to have on a regular basis...

[21] It is important to keep in mind that these are two quite distinct issues. A single fluid description is likely to break down before the basic field equations for conservation of momentum, mass, and energy become inadequate.

number of particules. “Reasonably large” is not trivial to define, but it would be very surprising if $N \sim 1\,\mathrm{cm}^{-3}$ would cut it[22].

Well, it turns out that while our fluid description may well be in trouble at 1 AU, our *single fluid* description has already broken down by then. Observational evidence for this comes from the fact that the kinetic temperatures of electrons, protons, and α particles differ significantly at the Earth's orbit (see Table 2.1). These develop because the thermal conductivities of these various species are not the same (mostly because $\kappa \propto 1/m$). What normally offsets the development of these temperature differences are collisions between the various species[23], which cause momentum and energy exchange. At what point do collisions become inefficient in redistributing thermal energy as fast as thermal conduction segregates it among the various species? The full answer involves a lot of kinetic theory, but again it is possible to get a feel for it using simple arguments. The time interval between collisions in a fully ionized hydrogen behaving as a single fluid is (for protons):

$$t_C \simeq 12 \frac{T^{3/2}}{N\, \ln \Lambda} \qquad [\mathrm{s}], \tag{2.26}$$

which for $N \sim 10\,\mathrm{cm}^{-3}$ and $T \sim 10^5\,\mathrm{K}$ gives $t_C \simeq 1.6 \times 10^6\,\mathrm{s}$, $\sim$ 20 days! In that time, a solar wind proton travels a distance $500\,\mathrm{km\,s}^{-1} \times 20$ days $\sim 10^9$ km. This means that a proton experiencing a collision near the earth's orbit will end up in the vicinity of Saturn by the time it is “due”, on the average, for its next collision! And that's assuming a constant particle density $N \sim 10\,\mathrm{cm}^{-3}$ beyond the Earth's orbit! Our single fluid model is actually doing surprisingly well, all things considered. But we can do better than that.

Problems

(2.1) Design a nozzle (i.e., compute and plot a $\sigma(x)$ function) that would yield the same isothermal flow profile than found here for the isothermal solar wind.

(2.2) Demonstrate that the accelerating transsonic solution represents a minimum energy solution, among all types of solutions on Fig. 2.2 that extend from r_0 to infinity.

(2.3) Construct a numerical solution corresponding to a class III isothermal solution (i.e., subsonic for all r, cf. Fig. 2.2). Provide plots of the flow speed, density,

---

[22] Hold it. So who ever said that the $\mathbf{x}$-part of a cell in phase space has to be one centimeter on a side ? So what if $N \sim 1\,\mathrm{cm}^{-3}$, I just make the $\mathbf{x}$-part of my cells in phase space 1 km on a side, say, and I'm on a roll again with a whopping 10^{15} particles to distribute in the $\mathbf{v}$-part of phase space... Is it really so ? What do you think limits the size of cells in phase space ?

[23] By “collisions” we do not imply billiard-type collisions, but rather deflections due to Coulomb interaction, of course.

and pressure as a function of r. Examine the asymptotic ($r \to \infty$) behavior of your solution. Discuss the physical relevance of your solution.

(2.4) This problem may seem a bit overwhelming at first, but stick to it and it all works out... The idea is to introduce an additional ingredient, *rotation*, in the Parker isothermal solution. As in this chapter work in spherical polar coordinates, and *restrict your solution to the equatorial plane.*

(a) obtain the equivalents of eqs. (2.10) and (2.13).
(b) Establish the location of the critical point(s) in your solution.
(c) Investigate the solution topology for various rotation rates. You may find useful to introduce a parameter $\zeta = \Omega r_0/a$. Provides plots equivalent to Fig. 2.2 for a few values of ζ. Do transsonic solutions exist for all values of ζ ?
(d) For $\Omega = \Omega_\odot$, $T_0 = 1.5 \times 10^6\,\mathrm{K}$ and $r_0 = 1.15\,R_\odot$, evaluate the flow speed and mass flux of your rotating solution. Compare this with the values obtained in this section for the non-rotating isothermal model. What do you conclude concerning the importance of rotation in modeling the solar wind ?

Bibliography

Parker's original paper is a great lesson in how to do good physics starting from simple assumptions, and should not be missed:

Parker, E.N. 1958, ApJ, 128, 664.

On circumstantial evidence for the present of a continuous outflow from the Sun, based on comet tail acceleration, see

Biermann, L. 1951, Z. Ap., 29, 274,

but note that Biermann's model has not withstood the test of time. We have briefly encountered the issue of the "termination" of the wind at large distances from the Sun, when the wind pressure becomes comparable to the pressure in the interstellar medium. This is actually a fascinating MHD problem. A recent review is

Holzer, T.E. 1989, ARA&A, 27, 199.

On the observational solar wind, some classical references are

Hundhausen, A.J. 1972, *Coronal Expansion and Solar Wind*, (Berlin: Springer), chap. 3.
Feldman, W.C., Asbridge, J.R., Bame, S.J., & Gosling, J.T. 1977, in *The Solar Output and its Variation*, ed. O.R. White (Boulder: Colorado Associated University Press), p. 351,

Table 2.2 herein being adapted from the latter. Note that the book by Hundhausen also discusses in detail a number of theoretical/modelling aspects. The *Pionneer 10* and *11*, as well as the *Voyager* probes, are still transmitting solar wind data from the edge of the solar system. Recent review of these data can be found in

> Grzedzielski, S., & Page, D.G. (eds.) 1990, *Physics of the outer Heliosphere* (Oxford: Pergamon Press).

Check out in particular the papers by Lazarus & McNutt (p. 229), Barnes (p. 235), and Smith (p. 253). Some *Ulysses* data are presented in

> Bame, S.J., Phillips, J.L., McComas, D.J., Gosling, J.T., & Goldstein, B.E. 1992, in *Solar Wind Seven*, E. Marsch, & R. Schwenn (Oxford: Pergamon Press).

While recent out-of-the-ecliptic *Ulysses* data are presented and discussed in, e.g.,

> Bame, S.J., Goldstein, B.E., Gosling, J.T., Harvey, J.W., McComas, D.J., Neugebauer, M., & Phillips, J.J. 1993, GRL 20, 2323.
> Gosling, J.T., Bame, S.J., McComas, D.J., Phillips, J.L., Pizzo, V.J., Goldstein, B.E., & Neugebauer, M. 1993, GRL 20, 2789.
> Phillips, J.L., Balogh, A., Bame, S.J., Goldstein, B.E., Gosling, J.T., Hoeksema, J.T., McComas, D.J., Neugebauer, M., Sheeley, N.R., & Wang, Y.-M. 1994, GRL 21, 1105.

There has been at least one *Ulysses* paper appearing almost every month in JGR or GRL over the past two years, so if you're interested in this stuff keep an eye out for papers by various linear combinations of these authors. Multi-fluid models have received particular attention in recent years. The paper that started it all is

> Hartle, R.E., & Sturrock, P.A. 1968, ApJ, 151, 1155.

Good (if technical) entry points in the recent literature are

> Cuperman, S., Tzur, I., & Dryer, M. 1984, ApJ, 286, 763
> Bürgi, A. 1992, JGR, 97, 3137
> Leer, E., Holzer, T.E., & Shoub, E.C. 1992, JGR, 97, 8183
> Hansteen, V.H., Leer, E., Holzer, T.E. 1994, ApJ, 428, 843

3. THERMALLY-DRIVEN WINDS: II. POLYTROPIC MODELS

"Science is experiment; science is trying things. It is trying each possible alternative in turn, intelligently and systematically; and throwing away what won't work, and accepting what will, no matter how it goes against our prejudices."

Jacob Bronowski
A Sense of the Future (1948)

The models constructed in the preceeding chapter suffer from a number of shortcoming, not the least of which is the asymptotic divergence of the flow velocity as $r \to \infty$. The latter can be directly traced to the assumption of *isothermality*. Our first step in constructing more realistic solar wind models is consequently to relax this assumption.

3.1 Basic polytropic wind model

As in §2.2, we consider a steady-state, non-rotating and unmagnetized spherically symmetric outflow, so that eqs. (2.5) and (2.7) remain unchanged. As before we assume that the temperature, density, etc. are known at some fiducial reference radius r_0 and will write $T_0 = T(r_0)$, etc. However, we now consider a *polytropic* model, i.e. one in which the pressure and density are assumed to be related by a relation of the form

$$\left(\frac{p}{p_0}\right) = \left(\frac{\rho}{\rho_0}\right)^{\alpha}, \tag{3.1}$$

with α constant and specified *a priori* (cf. §1.3) and $c_{s0}^2 = \alpha p_0/\rho_0$ is the sound speed at the reference radius. The sound speed now varies with r, viz.

$$c_s(r) = c_{s0}\left(\frac{\rho}{\rho_0}\right)^{\alpha-1} \tag{3.2}$$

Using as before the mass continuity constraint to eliminate the density, the r-momentum equation can now be manipulated into the form

$$\left[v_r^2 - c_{s0}^2 \left(\frac{v_{r0} r_0^2}{v_r r^2}\right)^{\alpha-1}\right] \frac{\partial v_r}{\partial r} = \frac{v_r}{r}\left[2c_{s0}^2 \left(\frac{v_{r0} r_0^2}{v_r r^2}\right)^{\alpha-1} - \frac{GM_\odot}{r}\right] \tag{3.3}$$

and/or integrated once to yield the Bernoulli equation

$$\frac{v_r^2}{2} + \frac{c_{s0}^2}{\alpha - 1}\left(\frac{v_{r0} r_0^2}{v_r r^2}\right)^{\alpha-1} - \frac{GM_\odot}{r} = E \tag{3.4}$$

which are the polytropic equivalents of eqs. (2.10) and (2.13). Note in particular that in the isothermal limit $\alpha \to 1$, $c_{s0} \to a$, eq. (3.3) reduces immediately to eq. (2.10). Clearly the quantity in square brackets on the LHS of eq. (3.3) vanishes when the flow speed becomes equal to the *local* sound speed, so that the RHS must simultaneoulsy vanish to avoid the appearance of a singularity. It is left as an exercise (cf. Problem 3.1) to show that the critical point r_s is located at

$$r_s = \left(\frac{1}{c_{s0}^2}\right)^{2/(5-3\alpha)} \left(\frac{GM}{2}\right)^{(\alpha+1)/(5-3\alpha)} \left(\frac{1}{v_{r0} r_0^2}\right)^{2(\alpha-1)/(5-3\alpha)}, \tag{3.5}$$

where

$$v_{rs} = c_s(r_s) = \left(\frac{GM}{2r_s}\right)^{1/2}. \tag{3.6}$$

So far things look somewhat messier but otherwise not very much different from the isothermal case. There exists a crucial difference, however. The location of the critical point can no longer be determined *a priori* from the input quantities c_{s0}, etc; computing r_s requires the knowledge of the base flow speed v_{r0}, which is *not* an input quantity.

Figure 3.1 illustrates the topology of a polytropic solution with $\alpha = 1.1$ and $T_0 = 1.5 \times 10^6$ K (which yields $c_{s0} \simeq 165\,\mathrm{km\,s^{-1}}$). Comparing this with Fig. (2.2), it is clear that the topology of this polytropic solution is very much similar to that of the isothermal solution. There is again a single solution that is accelerating and transsonic, which is the solution we identify with the solar wind.

The procedure used to construct a full solution (i.e., obtaining $v_r(r)$, $\rho(r)$, etc.) resembles that used in the isothermal case. We begin by evaluating the Bernoulli constant at r_0 and r_s:

$$E(r_0, v_{r0}) = \frac{v_{r0}^2}{2} - \frac{GM}{r_0} + \frac{c_{s0}^2}{\alpha - 1}, \tag{3.7}$$

$$E(r_s, v_{rs}) = -\frac{GM}{2r_s} + \frac{c_{s0}^2}{\alpha - 1}\left(\frac{v_{r0} r_0^2}{\sqrt{GM/2r_s}\, r_s^2}\right)^{\alpha-1}. \tag{3.8}$$

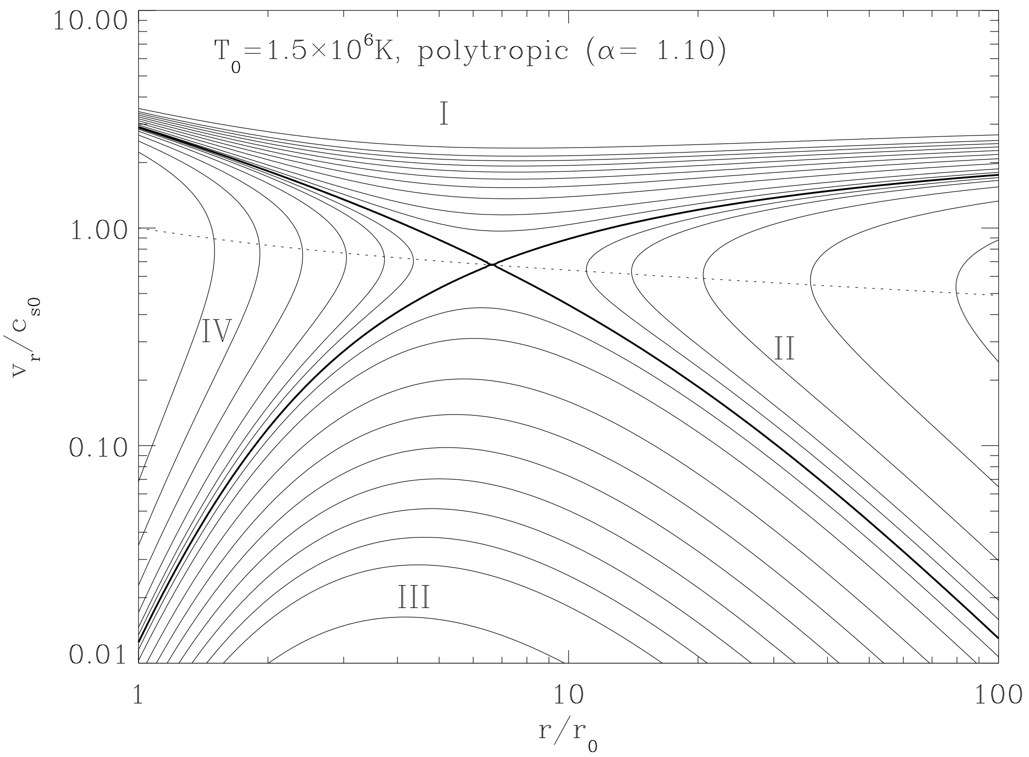

Figure 3.1: Topology of a polytropic wind solution ($\alpha = 1.1, T_0 = 1.5\times10^6$ K). As in the isothermal case of chapter 2 there is a single accelerating transonic solution that satisfies the boundary conditions as $r \to \infty$. The dotted line is the run of the sound speed with r.

Equating the RHSs of eqs. (3.7) and (3.8) yields once more a nonlinear root finding problem for v_{r0}. It is more complex than that treated in §2.2, since r_s is now itself a nonlinear function of v_{r0} The simple iterative scheme used in §2.2 no longer works so well for any α and c_{s0}. Time to face the music and admit that we are indeed confronted with a non-linear root finding problem that looks like

$$E(r, v_r) - E(r_0, v_{r0}) = 0. \tag{3.9}$$

How do we go about solving that ? A *very* accessible introduction to the numerical solution of such problems, is to be found in chapter 9 of the book *Numerical Recipes* (see bibliography). Possibly the simplest method is the so-called *Bisection Method.* Given a nonlinear function $f(x)$ and a range $[x_1, x_2]$ in which we seek a root x_r such that x_r is within within a (predetermined) absolute accuracy ε of the true root. A pseudocode for the bisection method would look something like this:

while $\delta \geq \varepsilon$ **do**
  $x_m = (x_1 + x_2)/2$
  if $f(x_2) \times f(x_m) \geq 0$ **then**

$x_2 = x_m$
else
$x_1 = x_m$
endif
$\delta = x_2 - x_1$
enddo

The nice thing about the bisection method is that it is *guaranteed* to find the root *if* a root indeed exists in the (preset!) interval $[x_1, x_2]$. Its chief drawback is that it converges linearly to the root, which, if high accuracy is required, can take a lot of iterations[1]. The *Newton-Raphson* method converges quadratically if some initial guess as to the position of the root can be made such that the guess is not too far away from the true root. "Not too far away" is unfortunately very ill-defined, and depends on the detailed behavior of the function involved. Here is a pseudocode for the Newton-Raphson method; all that is required is a starting guess x_0 at the root:

while $\delta \geq \varepsilon$ **do**
$x_r = x_0 - f(x_0) \times (\mathrm{d}f/\mathrm{d}x|_{x=x_0})^{-1}$
$\delta = |x_r - x_0|$
$x_0 = x_r$
enddo

Note that this algorithm requires the knowledge of $\mathrm{d}f/\mathrm{d}x$, which in the case of interest here translates into $\mathrm{d}E/\mathrm{d}v_r$. The basic assumption behing the Newton-Raphson method is that, as the root is approached, a Taylor series expansion truncated after the second term becomes an increasingly accurate representation of the true function in the (shrinking) interval $[x_0, x_r]$. However, in some apparently simple cases the Newton-Raphson method can behave in some truly disastrous ways; see for example Figs. 9.4.2 and 9.4.3 in the *Numerical Recipes* book [2]. The pseudocode given here should be complemented with a number of "safety checks"[3]. So the solution strategy is the following:

---

[1] How about using, for an absolute tolerance criteria, something like $f(x_r) \leq \varepsilon$? Can you think of cases where this is a superior criteria ? of cases where it is an inferior criteria ?

[2] I have to make a few personal editorial comments here:

(1) *Numerical Recipes* is a *great* place to learn basic scientific computing techniques and look for canned routines to do relatively simple things.
(2) *never* used any routine from *Numerical Recipes* (or anywhere else for that matter) without *first* thoroughly reading the *whole* corresponding chapter.
(3) Actually, unless absolutely unpractical, *always* write your own routines...

[3] Can you think of one ?

(1) For a given α and c_{s0}, solve the nonlinear root finding problem $E(r_0, v_{r0}) - E(r_s, v_{rs}) = 0$ for v_{r0} (you can now calculate r_s explicitely).
(2) Select a value of $r \neq r_0$
(3) Solve $E(r_0, v_{r0}) - E(r, v_r) = 0$ for for v_r (with r fixed).
(4) Select new value of r and repeat step (3) until flow profile is constructed (with adequate resolution) over the r-range of interest.

Problem 3.2 asks you to code in either of the above pseudocodes for the bisection or Newton-Raphson method, in the computing language of your choice, and reconstruct a polytropic flow solution $v_r(r)$[4][5]. Once this is known, it is straightforward to obtain expression for the density, pressure, and temperature profiles:

$$\frac{\rho(r)}{\rho_0} = \left[1 - \frac{(\alpha-1)GM}{r_0 c_{s0}^2}\left(1 - \frac{r_0}{r}\right) - \frac{(\alpha-1)}{2c_{s0}^2}\left(v_{r0}^2 - v_r^2\right)\right]^{1/(\alpha-1)}, \tag{3.10}$$

$$\frac{p(r)}{p_0} = \left[1 - \frac{(\alpha-1)GM}{r_0 c_{s0}^2}\left(1 - \frac{r_0}{r}\right) - \frac{(\alpha-1)}{2c_{s0}^2}\left(v_{r0}^2 - v_r^2\right)\right]^{\alpha/(\alpha-1)}, \tag{3.11}$$

$$\frac{T(r)}{T_0} = \left[1 - \frac{(\alpha-1)GM}{r_0 c_{s0}^2}\left(1 - \frac{r_0}{r}\right) - \frac{(\alpha-1)}{2c_{s0}^2}\left(v_{r0}^2 - v_r^2\right)\right]. \tag{3.12}$$

Compare these expressions with eqs. (1.36), (1.37) and (1.38). Figure 3.2 illustrates the variations with radial distance of the density, pressure and temperature for the $\alpha = 1.1$ polytropic solution of Fig. 3.1, together with the corresponding profiles for a $\alpha = 1.1$ polytropic static corona of identical base temperature (dotted lines). Within the sonic point $r = r_s$ the structure of the solution is very much like that of a static atmosphere, while for $r > r_s$ the solutions differ markedly. This is exactly the behavior we had encountered with the isothermal wind model. A detailed comparison with Fig. 2.5 reveals a somewhat lower base flow speed (v_{r0}), as well as a lower asymptotic flow speed at large distances. Examination of the force balance in the polytropic solution is carried out on Figure 3.3. The force

[4] All this seems like a lot of work; for each value of r we need to solve a nonlinear root finding problem. How about using a *shooting method*. In this context this would entail "guessing" a value for v_{r0}, using eq. (3.3) to estimate $\mathrm{d}v_r/\mathrm{d}r$ and step forward the solution, with an algorithm like

$$v_r(r + \Delta r) = v_r(r) + \frac{\mathrm{d}v_r}{\mathrm{d}r}\Delta r$$

Any idea why this may turn out to be more work than the procedure outlined above ?

[5] Even better, how about solving eq. (3.3) directly as a nonlinear two-point boundary-value problem. There are *scores* of numerical schemes out there that do exactly this...

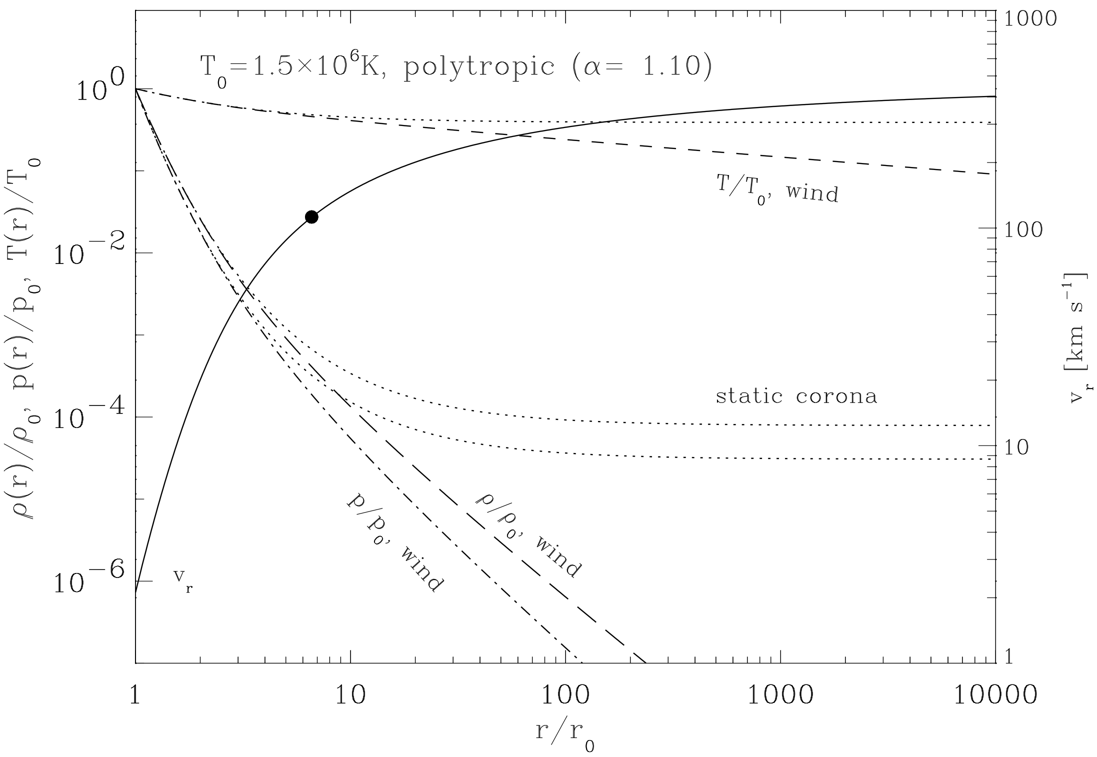

Figure 3.2: The full wind solution corresponding to the accelerating transsonic solution of Fig. 3.1. Dotted lines correspond to a polytropic static coronal model with identical α and T_0. The solid dot indicates the location of the sonic point.

balance is seen to be qualitatively similar to the isothermal case (cf. Figure 2.6). Upon closer scrutiny, you should be able to convince yourself that the asymptotic *slope* of the thermal acceleration term is not quite the same. This turns out to be a crucial difference between the isothermal and polytropic solutions, and we now turn to a more "in-depth" investigation of the causes (and consequences) of this difference.

3.2 Asymptotic behavior

From a pragmatic point of view, the first thing to note is that we are now dealing with a two-parameter family of solution. Whereas the isothermal wind model depended only on T_0, the polytropic solution depend on T_0 and α. Before we turn to asymptotics *per se* we should perhaps first ask ourselves whether or not there are regions in 2-D parameter space where transsonic wind solutions simply do not exist.

Doing once more something undoubtedly familiar by now, we equate $E(r, v_r)$ evaluate at r_0 and in the limit $r \to \infty$:

$$\frac{v_{r0}^2}{2} - \frac{GM}{r_0} + \frac{c_{s0}^2}{\alpha - 1} = \lim_{r\to\infty} \left[\frac{v_r^2}{2} - \frac{GM}{r} + \frac{c_{s0}^2}{\alpha - 1} \left(\frac{v_{r0} r_0^2}{v_r r^2} \right)^{\alpha - 1} \right]. \qquad (3.13)$$

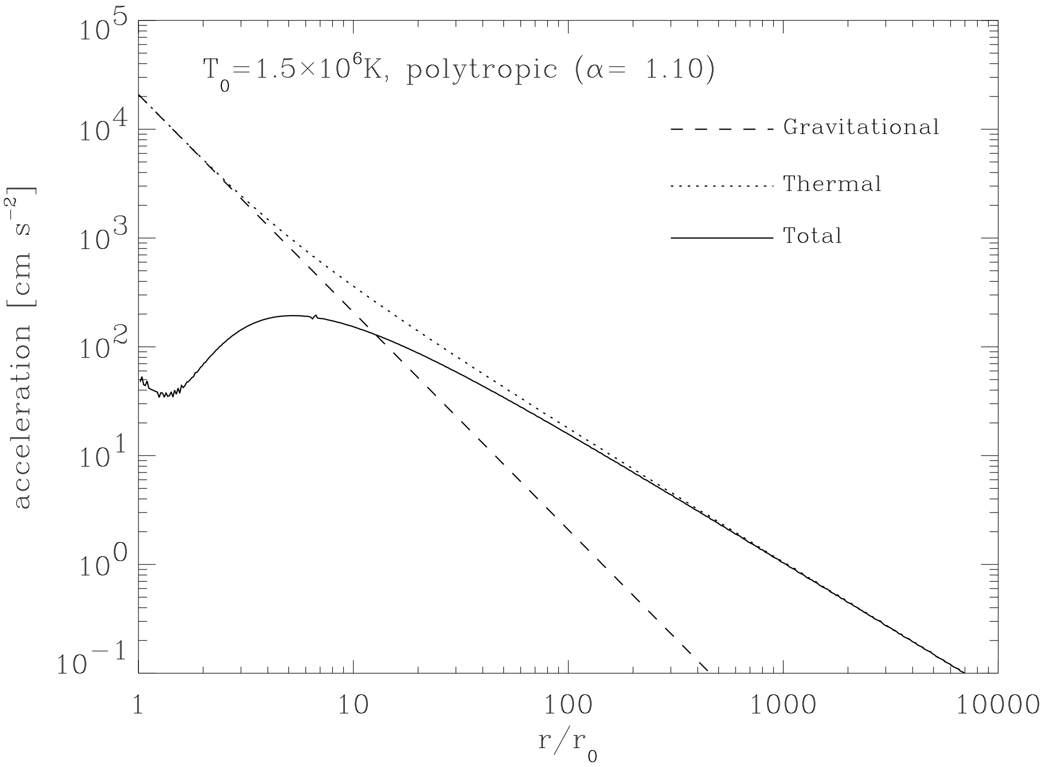

Figure 3.3: Force balance in the wind solution of Fig. 3.2.

Now $\lim_{r\to\infty}(1/r) \to 0$, $\lim_{r\to\infty} v_r \gg v_{r0}$, and and $\lim_{r\to\infty}(v_{r0}r_0^2/v_r r^2)^{\alpha-1} \to 0$ (because $\alpha - 1 > 0$). Equation (3.13) readily yields

$$\lim_{r\to\infty} v_r \equiv v_{r\infty} = \left(\frac{2c_{s0}^2}{\alpha-1} - \frac{2GM_\odot}{r_0}\right)^{1/2}. \tag{3.14}$$

Note that this is a finite number, a constant (i.e., no r dependency). You will recall that while the isothermal wind solutions of §2.2 took care of the non-vanishing asymptotic pressure problem that plagued the static coronal models of §1.4, they produced a new problem of their own, namely that logarithmically diverging flow velocity in the asymptotic limit $r \to \infty$. Our new and improved polytropic solutions certainly seem to have taken care of *that* problem.

Clearly all wind solutions must have $v_{r\infty} > 0$ for finite r, so that we have the constraint[6]:

$$\frac{c_{s0}^2}{\alpha-1} - \frac{GM_\odot}{r_0} \geq 0. \tag{3.15}$$

[6] Why is that so ? What's wrong with a steady, spherically symmetric wind accelerating in the corona and then, at some large distance, deccelerating again until everything grinds to a full stop ?

For $\alpha = 1.1$, this requires that $T_0 \gtrsim 9 \times 10^5\,\mathrm{K}$. Again you will recall that the isothermal solutions had the annoying characteristic that transsonic wind solutions could be constructed all the way into the limit $T_0 \to 0$, which, we argued, was kind of troubling, intuitively and physically. For an accelerating transsonic solution, it seems reasonable to require that $\mathrm{d}v_r/\mathrm{d}r > 0$ near the base of the flow. Going back to eq. (3.3), this implies

$$2c_{s0}^2 - \frac{GM_\odot}{r_0} < 0, \tag{3.16}$$

requiring that $T_0 \lesssim 5 \times 10^6\,\mathrm{K}$. So a transsonic wind can only exist for a base temperature in the range

$$\left(\frac{\alpha - 1}{\alpha}\right) \frac{GM_\odot \mu m}{kr_0} \leq T_0 < \left(\frac{1}{2\alpha}\right) \frac{GM_\odot \mu m}{kr_0} \tag{3.17}$$

Recognize this ? This looks very much like the infamous middle ground between light, and shadow; this is the area which, in §1.4, we called... The Twilight Zone... Everything fits ! It's a miracle !! Alleluiah Hosannah Banzai !!!

Ahem. Excuse me. Let's carry on. What do these two bounds on T_0 correspond to ? The lower bound, it turns out, is indeed the elusive criteria for a gravitationally bound/unbound atmosphere that we were after when we put eq. (1.41) down on paper ! We had it already, it turns out, in the form of eq. (1.39). The upper bound is something new. It represents the temperature above which steady, transsonic wind-like solutions no longer exist. If this criterion were to be violated (e.g. by a sudden increase in base temperature), the whole atmosphere would "explode" outward supersonically. This, in fact, is the kind of criterion we were after in setting down eq. (1.41). So we learned something.

There is something else that is extremely important that can be extracted from eq. (3.17); if there is to be a finite temperature interval over which eq. (3.17) is to be satisfy, then we *must* have $\alpha > 3/2$. Otherwise both criteria cannot be satisfied simultaneously. We therefore have the additional constraint

$$1 \leq \alpha \leq \frac{3}{2}, \tag{3.18}$$

independently of the assumed base temperature T_0 ! Compare this with the thermodynamically (so to speak) allowed range of α (cf. eq. [1.23]).

Figure 3.4 illustrates, in the $[T_0, \alpha]$ plane, the region in parameter space that allows the existence of steady, transsonic solutions. The thermodynamically allowed bounds on α ($1 \leq \alpha \leq 5/3$) restrict solutions to the region located *below* the dotted line. Equation (3.15) (finite asymptotic flow velocity) restricts solutions to the *right* of the dash-dotted line. Equation (3.16) (subsonic, accelerating flow at r_0) restricts solutions to the *left* of the dashed line. So our allowed region is clearly region II. Region I is that of steady coronae of finite radial extent, discussed in §1.4; and in region III no steady wind-type solutions are possible[7].

---

[7] So what is happening in region IV then ?

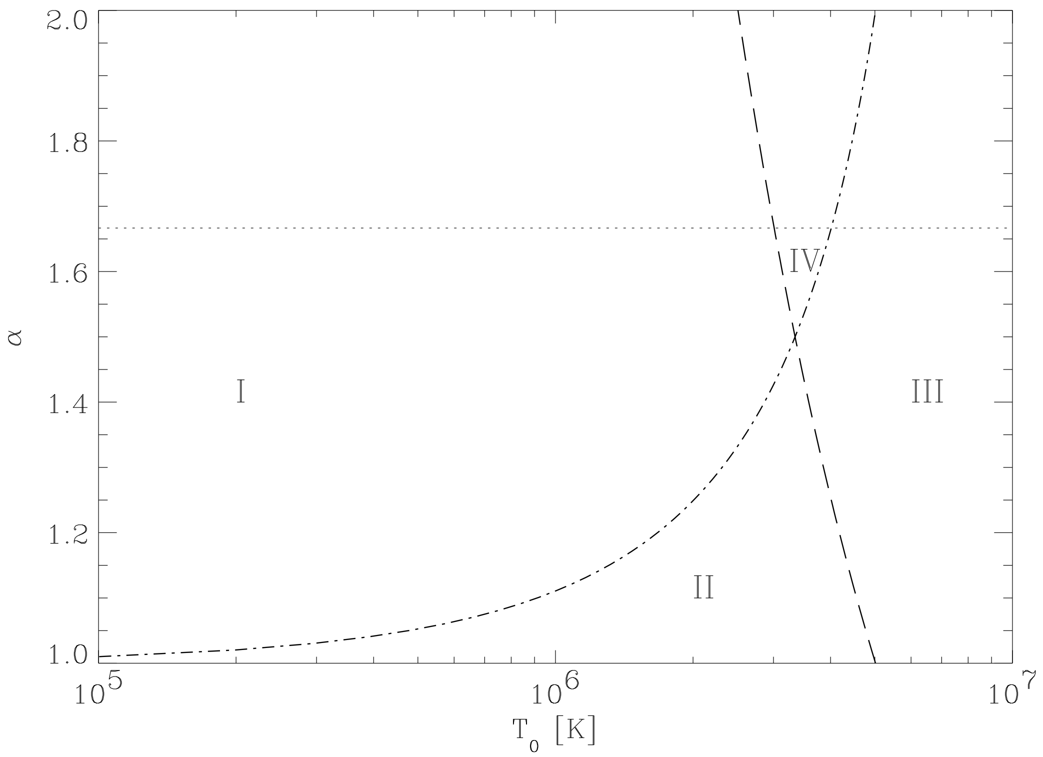

Figure 3.4: Allowed region in the $[T_0, \alpha]$ for the existence of steady, transsonic polytropic wind solutions. The region above the dotted line has $\alpha > 5/3$, and so is excluded "thermodynamically" (cf. §1.3). Region II is the allowed region defined by eq. (3.17) (see text).

Further insight into these restrictions can be obtained by examining the topologies of a few "illegal" solutions, i.e., solutions with $\alpha \geq 3/2$. This is carried out on Figure 3.4, again for $T_0 = 1.5 \times 10^6$ K. The top panel is a borderline solution with $\alpha = 3/2$. There exists a constant velocity, transsonic solution[8]. For higher values of α [bottom panel], there still exists two transsonic solutions, but they are *both* supersonic at r_0 and deccelerating for all r. Clearly these are no acceptable wind solutions. In the limit $\alpha \to 5/3$ these solutions actually have $v_{r0} \to \infty$.

3.3 Energetics

You will undoubtedly recall from §1.3 that buried deep in the polytropic approximation (i.e., eq. [3.1] with α a constant specified *a priori*) is a very specific energy source/sink functional form. We now have pretty good solution, in terms of its asymptotic behavior, etc., but must now ask ourselves whether or not this solution involves distributions of energy sources/sinks that are even mildly reasonable.

[8] How can it be constant velocity *and* transonic ????

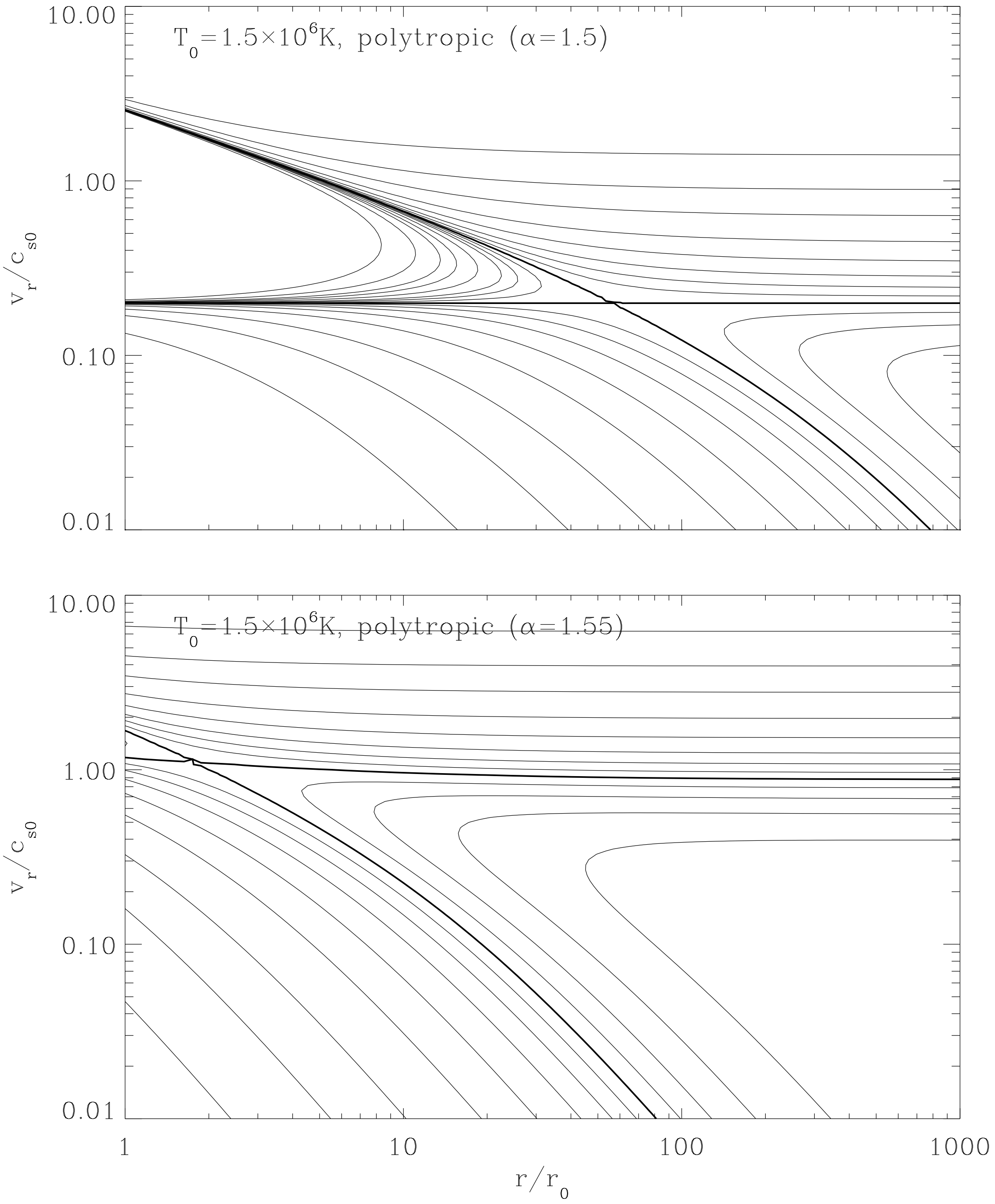

Figure 3.4: Topology of polytropic solutions having $\alpha \geq 3/2$. The top panel is a borderline solution with $\alpha = 3/2$. The bottom panel is a truly "illegal" solution.

Now our solutions, in general, will not satisfy the energy equation because the sources/sinks implicitly present in our models are not included in eq. (1.3). But we can turn the issue around and use our solution to determine what sources/sinks should appear on the RHS of the energy equation in order for our solution to satisfy eq. (1.3). Neglecting thermal conduction and limiting ourselved to steady-state ($\partial/\partial t = 0$) systems, the energy equation can be manipulated into the form

$$\nabla \cdot \left[\rho \mathbf{v} \left(\frac{1}{2} ||\mathbf{v}||^2 + \frac{3}{2} \frac{p}{\rho} \right) \right] + \nabla \cdot (p \mathbf{v}) - \rho \mathbf{v} \cdot \nabla V = 0. \tag{3.19}$$

Our solutions do not satisfy this equation, in the sense that substituting our solutions on the LHS does not return zero. Write instead

$$\nabla \cdot \left[\rho \mathbf{v} \left(\frac{1}{2} ||\mathbf{v}||^2 + \frac{3}{2} \frac{p}{\rho} \right) \right] + \nabla \cdot (p \mathbf{v}) - \rho \mathbf{v} \cdot \nabla V = s(r), \tag{3.20}$$

where $s(r)$ is our source/sink term (which has units of erg s^{-1} cm^{-3}). Direct substitution of our polytropic solutions on the LHS of this expressions allows to calculate directly the functional form of $s(r)$. The result is shown on Fig. 3.6, for a sequence of solution having $T_0 = 1.5 \times 10^6$ K. The *total* energy input associated with our sources/sinks is

$$S(\alpha, T_0) = 4\pi \int_{r_0}^{\infty} s(\alpha, T_0; r) r^2 \mathrm{d}r. \qquad [\text{erg s}^{-1}] \tag{3.21}$$

Carrying out this integrates yields $S = 1.1 \times 10^{28}$, 2.3×10^{27}, and 8.7×10^{26} erg s^{-1} for $\alpha = 1.05$, 1.1, and 1.15 respectively; in all cases less than 10^{-5} of the solar luminosity, a fortunate state of affairs.

3.4 Another comparison with the "real" solar wind

Time to compare our polytropic solutions to the real solar wind. Flow properties at 1 AU for the solution of Fig. 3.2 are listed in Table 3.1 below. Compare this to Table 2.1, in particular to the flow properties of low speed streams. Pretty amazing; our model values are within the observed fluctuations for the flow speed, *and* particle number density. We are off by a whopping factor of 10 on the temperature (the proton temperature should be the meaningful one to compare to in the context of our single-fluid models), but the fact that the observed temperatures for protons, electrons and Helium nucleii differ by large factors (cf. Table 2.1) is telling us (very loudly) something about the breakdown of our single fluid approximation.

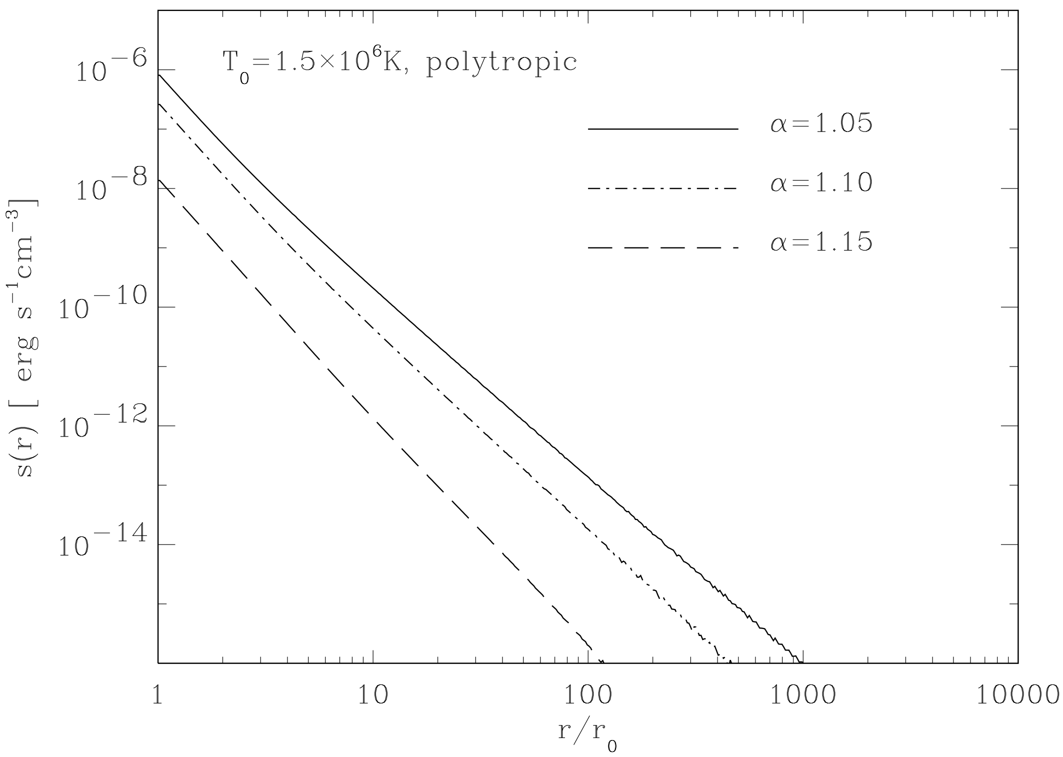

Figure 3.6: Energy input implicit in the polytropic wind solutions, for a few values of α.

Table 3.1

Properties of polytropic solution for $T_0 = 1.5 \times 10^6$ K, $\alpha = 1.1$, and $N_0 = 10^8 \text{cm}^{-3}$

r	v_r [km s^{-1}]	N [cm^{-3}]	T [K]
r_0	2.1	10^8	1.5×10^6
r_s	113	4×10^4	6.8×10^5
$r_\oplus$	315	16	3.1×10^5
$10\, r_\oplus$	377	0.12	1.9×10^5

It should also be pretty clear that we have gotten farther away from high speed streams, compared to our first isothermal solution. Within the framework of the thermally-driven models discussed above (both isothermal and polytropic), a large increase in the asymptotic flow velocity can only be generated by increasing the base temperature. This being generally ruled out by observations, a number of authors have attempted to "speed up" the solar wind at 1 AU. One way of doing so is by introducing additional sources of energy and/or momentum at various distances from the base of the corona. This can be mediated by outward propagating acoustic and/or magnetoacoustic and/or Afvén waves. An important result in that context is that

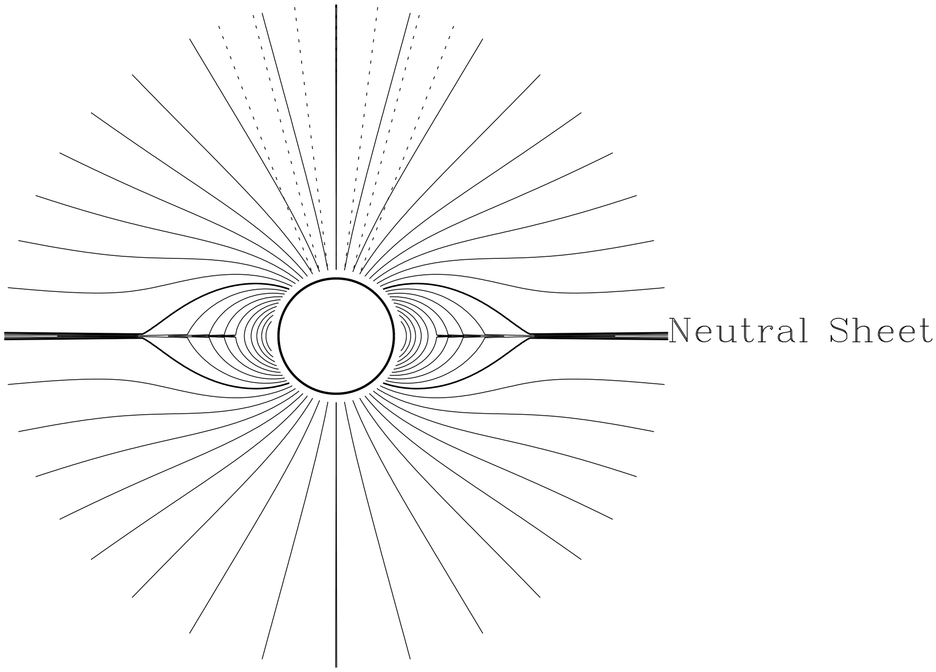

Figure 3.7: Schematic representation of the large-scale coronal magnetic field, applicable to solar minimum conditions if we don't look too closely at things. The dotted lines indicate purely radial expansion factors; note how in the polar regions the fieldlines diverge more rapidly than r^2 at first. This is an analytical force-free model developed by B.C. Low (1986, ApJ 310, 953).

- Adding momentum or energy in the subsonic ($r < r_s$) region increases the overall mass flux, but not the flow speed at 1 AU.
- Adding momentum or energy in the supersonic ($r > r_s$) region increases the flow speed at 1AU, but not the overall mass flux.

Another possibility is to construct wind models for high-speed streams where the geometrical expansion factor increases faster than r^2. The physical justification for this is that in the low-β plasma of the lower corona, the plasma is effectively channelled by the magnetic field, and the latter would only yield radial (i.e., $\propto r^2$) expansion factors for a purely monopolar magnetic field. For a dipolar field, the geometrical expansion factor increases more rapidly than r^2 in the polar regions. Eventually, the plasma β becomes larger than one[9]; the plasma then takes over the control of the system, and the magnetic field is forced opened in the equatorial regions, and a split-monopolar configuration results, with radial expansion factors.

[9] How's that ?! the pressure is falling pretty fast with distance, so how can the plasma β become larger than one ?

This is illustrated schematically on Fig. 3.7. Clearly, at high latitudes magnetic fieldlines diverge faster than r^2. Allowing for these variations in effective cross-section can speed up the wind, mostly in the coronal holes themselves but also, to a lesser extent, at 1 AU. Problem (3.5) asks you to explore this possibility for non-radial expansion factors having a specific functional form that qualitatively mimics the behavior seen in the polar regions on Fig. 3.7.

Problems

(3.1) Obtain eqs. (3.5) and (3.6) on your own.

(3.2) Code in the pseudocode for the bisection method, as given in the text, to reconstruct (and plot) a full polytropic wind solution (i.e. $v_r(r)$, $\rho(r)$, $p(r)$ and $T(r)$). Adopt values of α and T_0 *different* from those used to produce the solution shown on Fig. 3.2. And please do provide a listing of your code.

(3.3) If you have already done Problem 2.3 this one will probably seem familiar... And if you have done Problem 3.2, it may even be easy... Using e.g. the procedure outlined in the text, construct a numerical solution corresponding to a class III polytropic solution (i.e., subsonic for all r, cf. Fig. 3.1; use also $\alpha = 1.1$ and $T_0 = 1.5 \times 10^5$ K). Provide plots of the flow speed, density, pressure and temperature as a function of r. Examine the asymptotic ($r \to \infty$) behavior of your solution, and discuss its physical relevance.

(3.4) Obtain an expression for the asymptotic ($r \to \infty$) flow velocity for the polytropic wind models (i.e., equation [3.14]).

(3.5) The aim of this problem is to get you to construct a polytropic wind solution for non-radial expansion factors. Consider (and, while you're at it, plot) the following function

$$f(r; R_e) = \left(\frac{1}{r^2} + \frac{R_e}{r^3} \right)^{-1}$$

for $R = 1$, 2 and 10. Clearly we have $\lim_{r\to 0} f(r) \propto r^3$, and $\lim_{r\to\infty} f(r) \propto r^2$, with the "turning point" occurring at $r \sim R_e$. Qualitatively, this is the kind of behavior we would get from constructing expansion factors in the polar regions of the configuration shown on Fig. 3.7. Using this expansion factor, construct a few polytropic solutions with $T_0 = 1.5 \times 10^6$ K (e.g., consider $\alpha = 1.05$, 1.1, 1.15, etc.) and compare the resulting flow speed and densities at 1 AU with the solar wind data for high speed streams (cf. Table 2.2). Can you generate high speed stream in this way ?

Bibliography

Polytropic (as opposed to isothermal) wind solutions, together with their associated energy requirements, are presented in great detail and critically discussed in

Parker, E.N. 1963, *Interplanetary Dynamical Processes* (New York: John Wiley), chap. 6 and 7,

but the whole book is well worth reading cover to cover! The effect of additional energy/momentum sources in the corona on the solar wind speed is investigated in

Leer, E., & Holzer, T.E. 1980, JGR, 85, 4681

As an specific example of the effects of momentum deposition by waves as means of further accelerating thermally-driven winds, you may want to check out the following review, concerned with the dynamical effects associated with the propagation of Alfvén waves and written in a pretty pedagogical style (ask me for as copy):

MacGregor, K.B., & Charbonneau, P. 1997(?), in *Cosmic Winds and the Heliosphere*, eds. J.R. Jokipii, C.P. Sonnet, & M.S. Giampapa, (Tucson: The University of Arizona Press), in press.

A particularly interesting class of solar wind models with non-radial geometric expansion is developed and discussed in

Kopp, R.A., & Holzer, T.E. 1976, SolP, 49, 43

Full coordinates for the book *Numerical Recipes* mentionned in §3.1 are

Press, W.H., Flannery, B.P., Teukolsky, S.A., & Vetterling, W.T. 1986, *Numerical Recipes. The Art of Scientific Computing* (Cambridge: Cambridge University Press) [second ed. 1992].

Note that three versions of the book exist; they differ mainly (but not only) in the programming language used for the code listings provided in the book (you can choose from FORTRAN, PASCAL and C). The chapter and Figure numbers quoted in the text refer to the first edition.

4. ROTATING, MAGNETIZED, THERMALLY-DRIVEN WINDS

MÖBIUS: ...Sie dürfen beruhigt sein, Schwester Monika. Es ist nun alles in Ordnung.
SCHWESTER MONIKA: Sie handelten planmäßig.
MÖBIUS: Ich bin Physiker.

Friedrich Dürrenmatt
Die Physiker (1962)

This section deals with the introduction of two additional "ingredients" in the thermally-driven transonic wind solutions studied in the preceeding sections: rotation and magnetic fields. While it is not clear if these are essential ingredients in the winds of *all* stars, they are certainly important in the case of the solar wind. This is mostly due to the special way in which rotation and magnetic fields can interact, in the flow of a highly conducting plasma.

4.1 Flux freezing and the high electrical conductivity limit

Before attempting to construct a simple model of magnetized winds, there is an important concept that needs to be discussed: *flux freezing.* The starting point of our discussion is the notion of *magnetic flux* through a surface element dA in a moving, magnetized fluid. We can define this as

$$\Phi_B = \int_A \mathbf{B}\cdot\mathbf{n}\,\mathrm{dA}, \tag{4.1}$$

where $\mathbf{n}$ is a unit vector normal to dA. Consider now the *total* time-derivative of this quantity. The fluid being in motion, we must in general writes

$$\frac{\mathrm{d}\Phi_B}{\mathrm{d}t} = \frac{\mathrm{d}}{\mathrm{d}t}\int_A \mathbf{B}\cdot\mathbf{n}\,\mathrm{dA}$$

$$= \int_A \frac{\mathrm{d}\mathbf{B}}{\mathrm{d}t}\cdot\mathbf{n}\,\mathrm{dA} + \int \mathbf{B}\cdot\frac{\mathrm{d}}{\mathrm{dt}}(\mathbf{n}\mathrm{dA}) \tag{4.2}$$

since our surface element A will in general get deformed as it gets advected by the fluid motion. This latter quantity is in fact $\mathbf{v}\mathrm{d}t \times \mathrm{d}\ell$, where $\mathrm{d}\ell$ is an arc element along the circuit enclosing $\mathrm{d}A$[1]. We can thus write

$$\int \mathbf{B} \cdot \frac{\mathrm{d}}{\mathrm{d}t}(\mathbf{n}\mathrm{dA}) = \oint \mathbf{B} \cdot (\mathbf{v} \times \mathrm{d}\ell) \tag{4.3}$$

Using the vector identity $\mathbf{A} \cdot (\mathbf{B} \times \mathbf{C}) = (\mathbf{A} \times \mathbf{B}) \cdot \mathbf{C}$ and Applying Stokes theorem to the RHS of this expression, we can write equation (4.2) as

$$\frac{\mathrm{d}\Phi_B}{\mathrm{d}t} = \int_A \left[\frac{\mathrm{d}\mathbf{B}}{\mathrm{d}t} + \nabla \times (\mathbf{B} \times \mathbf{v}) \right] dA. \tag{4.4}$$

Compare the integrand to the induction equation [eq. (1.11), remembering that it was obtain in the limit $\eta \to 0$, or, equivalently, in the limit $\sigma_e \to \infty$]. This then leads to $\mathrm{d}\Phi_B/\mathrm{d}t = 0$. We conclude that in a highly conducting plasma, the magnetic field is *frozen* in the plasma, in the sense that the magnetic flux is carried along with the fluid as the latter moves. The only fluid motions that are not constrained by the magnetic field are then fluid motions directed entirely *along* fieldlines (because if $\mathbf{n}\mathrm{d}A$ is perpendicular to $\mathbf{B}$ the magnetic flux vanishes by definition. Alternately, it is clear from the induction equation that if $\mathbf{v}$ and $\mathbf{B}$ are parallel, the fluid motions do not affect the magnetic field).

Formally, the flux-freezing condition holds only in the strict limit $\eta \to 0$ (or, equivalently, $\sigma_e \to \infty$). Are there conditions under which $\eta \neq 0$, yet the flux-freezing approximation can be expected to hold to a high degree of accuracy? Insight into this question can be obtained via a simple order-of-magnitude argument. Replace, in the induction equation, ∇ by $1/\ell$, and $\mathbf{v} \times \mathbf{B}$ by $||\mathbf{v}||\mathbf{B}$:

$$\frac{\partial \mathbf{B}}{\partial t} = \frac{||\mathbf{v}||\mathbf{B}}{\ell} - \frac{\eta \mathbf{B}}{\ell^2}. \tag{4.5}$$

The ratio of the first to second term on the RHS is the *Magnetic Reynolds number*:

$$R_m = \frac{||\mathbf{v}||\ell}{\eta}. \tag{4.6}$$

Clearly, if $R_m \gg 1$ then the diffusive term makes a negligible contribution to the RHS of the induction equation, which means that flux-freezing is effectively enforced. For a corona composed of fully ionized hydrogen, we have

$$\sigma_e \simeq 2 \times 10^7 T^{3/2} \qquad [\mathrm{s}^{-1}], \tag{4.7}$$

[1] Can you figure that one out? Hint: make a drawing!

so that

$$\eta = \frac{c^2}{4\pi\sigma_e} \simeq 3.6\times 10^{12} T^{-3/2} \qquad [\mathrm{cm^2\,s^{-1}}], \tag{4.8}$$

which for $T \sim 10^6$ K yields $\eta \sim 10^4\,\mathrm{cm^2\,s^{-1}}$. Assuming $\ell \sim R_\odot$ and $||\mathbf{v}|| \sim 1\,\mathrm{km\,s^{-1}}$, the magnetic Reynolds number is $\sim 10^{12}$. That the Reynolds number is so large here is not so much that the resistivity is so small in the solar corona (it is actually rather large), but rather that the dimensions involved, of order $R_\odot$, are so large. Consequently, we must exercise care when applying the flux-freezing approximation in modelling structures evolving on small spatial scales.

What happens in the absence of any fluid motion? Then obviously $R_m = 0$ by definition, and dissipative effects, however small, dominate the magnetic field evolution. We must then retain the dissipative terms in the induction equation. In this limit, and for a constant η, the induction equation becomes simply[2]

$$\frac{\partial \mathbf{B}}{\partial t} = \eta\nabla^2\mathbf{B}. \tag{4.9}$$

Were it not from the fact that $\mathbf{B}$ is a vector, as opposed to scalar quantity, this would look very much like a simple heat diffusion equation. The timescales over which $\mathbf{B}$ is expected to vary can again be estimated using an order-of-magnitude argument, by again replacing ∇ by $1/\ell$ and $\partial/\partial t$ by $1/\tau$, to obtain:

$$\tau = \frac{\ell^2}{\eta}. \tag{4.10}$$

This is the timescale over which a magnetic field will dissipatively leak out of a conductor of typical dimensions ℓ. As an illustrative example, consider a large-scale magnetic field imbedded in the solar interior (for which again $\eta \sim 10^4\,\mathrm{cm^2\,s^{-1}}$). For $\ell \sim R_\odot$, eq. (4.10) yields $\tau \sim 10^{10}$ yr, about the same as the main-sequence lifetime of the Sun[3].

The bottom line of all this is that in constructing magnetized solar wind models, we will neglect magnetic dissipation. This means that we will use, instead of the full induction equation (1.11), the following expression:

$$\frac{\partial \mathbf{B}}{\partial t} = \nabla\times(\mathbf{v}\times\mathbf{B}) \tag{4.11}$$

---

[2] Show it.

[3] It may be appropriate at this juncture to point out that dynamo theory —the topic of part IV of this class— is not required to explain the existence *per se* of the solar magnetic field, but rather to explain the numerous peculiarities and short timescales ($\ll \tau$) of its temporal evolution. We will also revisit the diffusive decay of magnetic fields in part IV of the class.

4.2 Magnetic fields in the solar wind: observational aspects

Before going into actual observations of the interplanetary magnetic field, it is instructive to first try to "predict", on the basis of what we have already learned, what such a field should look like. More specifically, we consider a steady-state situation whereby

(1) Flux-freezing is effectively enforced,

(2) Magnetic stresses are neglected in the force balance,

(3) The poloidal part of the magnetic field is purely radial in the equatorial plane, with the field strength known at the reference radius.

In view of (3), the constraint $\nabla \cdot \mathbf{B} = 0$ yields a second order ODE which has a solution[4] of the form

$$B_r(r) = B_{r0}\left(\frac{r_0}{r}\right)^2 . \tag{4.12}$$

For an average surface field $B_0 \sim 1$ Gauss, eq. (4.12) yields $B_r \simeq 2.5 \times 10^{-5}$ Gauss at the Earth's orbit, which, wouldn't you know, is pretty close to the observed average magnetic field at 1AU. In view of (1), the flow streamlines coincide with magnetic fieldlines. In the absence of rotation, the Parker solution is immediately applicable. Consider now a situation where rotation at a rate $\Omega_\odot$ is present, at a rate such that centrifugal effects do not affect significantly force balance in the r-direction (you already know how and when this can happen, if you have already done problem [2.4], that is...). In a frame co-rotating with the Sun, the wind still flows along the magnetic fieldlines. But in a stationary frame, the total velocity is now

$$\mathbf{v} = \mathbf{v}' + \Omega\, r\, \hat{\mathbf{e}}_\phi, \tag{4.13}$$

where primed quantities refer to quantities evaluated in the co-rotating frame. In general, the magnetic fieldlines are thus defined by the spiral $r = (v/\Omega_\odot)(\phi - \phi_0)$, with the components of the magnetic field given by

$$B_r(r,\theta,\phi) = B_r(r_0,\theta,\phi - r\Omega_\odot/v_r)\left(\frac{r_0}{r}\right)^2 , \tag{4.14a}$$

$$B_\theta(r,\theta,\phi) = 0, \tag{4.14b}$$

$$B_\phi(r,\theta,\phi) = B_r(r_0,\theta,\phi - r\Omega_\odot/v_r)\left(\frac{r_0\Omega_\odot}{v_r}\right)\left(\frac{r_0}{r}\right) . \tag{4.14c}$$

Figure 4.1 shows, in the equatorial plane, the magnetic fieldlines defined by eqs. (4.14), with the dashed circle corresponding to the Earth's orbit[5]. The angle between a magnetic fieldline and the Sun-Earth radial segment is:

$$\phi_B = \arctan\left(\frac{B_\phi}{B_r}\right) = \arctan\left(\frac{r\Omega_\odot}{v_r}\right) , \tag{4.15}$$

[4] Obtain it.

[5] On Fig. 4.1, is the Sun rotating clockwise or counterclockwise ?

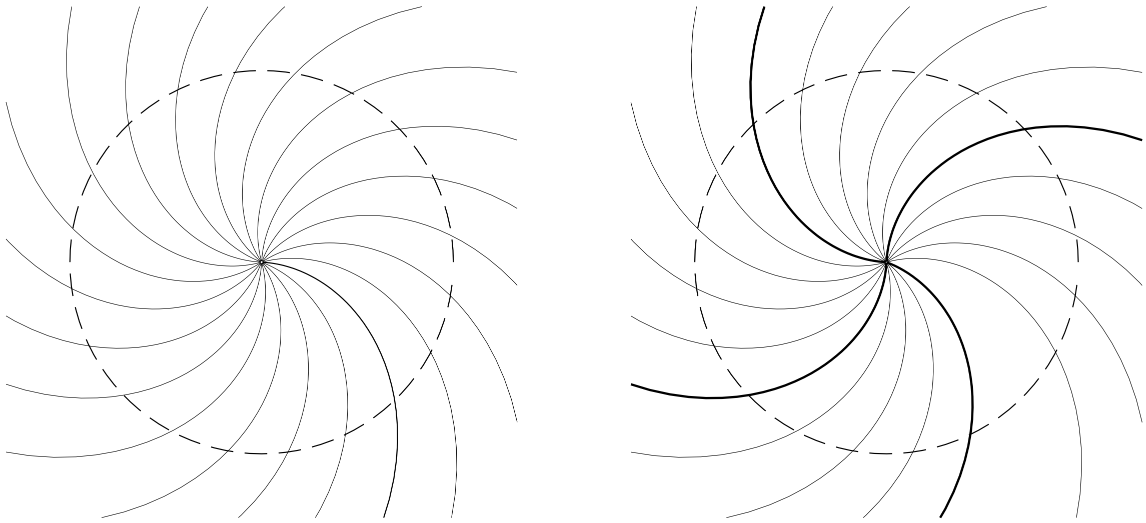

Figure 4.1: [Left] The spiral drawn by the solar magnetic field, as it is advected outward by the solar wind. Solid lines corresponds to magnetic fieldlines, and the circular dashed line to the Earth's orbit. The wind itself flows radially outward from the Sun (located at the center of the spiral, of course). [Right] Explanation for the observed magnetic polarity reversals in terms of magnetic sectors. Polarity changes occur when the dividing line between two sector (thicker lines) rotates past the Earth.

which at 1 AU gives the rather large value $\phi_B \simeq 55^o$. The net wind velocity, as observed from the Earth, on the other hand, is essentially radial[6].

Observationally, there is one important feature of the solar wind's magnetic field that need further discussion. Spacecraft observations at the Earth's orbit reveal the presence of fairly rapid polarity reversals in the observed magnetic field, after which the polarity remains the same for periods of days before undergoing the next reversal. That these reversals often exhibits a 28 days periodicity is a strong indication that they are associated with the rotation of large-scale magnetic structure co-rotating with the Sun. These have been named *magnetic sectors*. Their theoretical interpretation lead to some level of controversy. The most straightforward interpretation is that we are "seeing" regions of opposite polarities on the Sun, extended outward by the solar wind. This is illustrated on Figure 4.1 (right panel). Polarity reversal occur when the boundary between two sectors (thicker lines) zooms by the Earth, in a lighthouse sort of way.

What this means in term of the large-scale magnetic field structure in the solar corona is a different issue. Remembering that the ecliptic and the Sun's equatorial plane subtend an angle of $\sim 7^o$, the question arises as to whether we

[6] Confusion on the horizon. Didn't we argue that in the flux-freezing limit, the gas could only flow parallel to the fieldlines ? Shouldn't we than have $\arctan(v_\phi/v_r) \simeq 55^o$ also ? How do you explain this ?

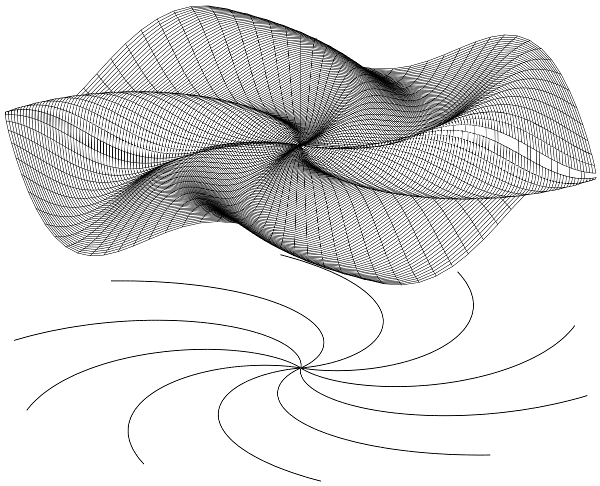

Figure 4.2: The neutral sheet of the Sun's extended magnetic field. The magnetic axis is in the vertical direction, and essentially coincides with the rotation axis. As the Sun rotates, we see alternately above and below the neutral sheet. The thicker lines on Fig. 4.1 are then the intersection of the neutral sheet with the equatorial (ecliptic) plane.

are seeing large-scale magnetic structures of opposite polarities, of high latitudinal extent and distributed in longitude along the equator. The answer is no. At times of solar minimum at least, the solar coronal magnetic field exhibits an overall dipolar structure, looking very much like Fig. 3.7 actually. Close to the Sun, this means $B_r = 0$ in the equator, but farther away, there is a neutral sheet in the equatorial plane, separating regions of opposite polarities (i.e., $\pm B_r$) above and below. If the neutral sheet was strictly planar, given the 7^o difference between the Sun's rotation axis and the Earth's orbital axis, we could see at most 2 polarity reversals per solar rotation (instead we see something like 4—6). The reason is that the neutral sheet is warped, allowing us to "see" above and below more often per rotation cycle. This is illustrated on Fig. 4.2.

The warping of the neutral sheet can be traced all the way back down to the solar photosphere. Even at times of minimum activity, where the corona assumes a globally dipolar structure (cf. Fig. 3.7), it is never exactly dipolar. Consequently, the photospheric neutral line (that's the line on the photosphere where $B_r = 0$) never coindides exactly with the solar equatorial plane.

The above discussion has allowed us to draw a picture of the interplanetary magnetic field which, qualitatively, is quite accurate. But if we want to be more quantitative (i.e., provide estimates for things such as the angular momentum loss rate), we must take into account the effect of magnetic stresses on the large-scale wind dynamics. This is the topic to which we now turn.

4.3 The Weber-Davis solution

As in the rotating, non-magnetized wind case treated previously, we seek steady-state ($\partial/\partial t = 0$), axisymmetric ($\partial/\partial\phi = 0$) solutions in the equatorial plane ($\partial/\partial\theta = 0$ and $v_\theta = 0$). We further assume that the symmetry axis of the magnetic field coincides with the rotation axis, and that the magnetic field is symmetric with respect to the equatorial plane (i.e., $B_\theta = 0$). In other words, we have $\mathbf{v} = (v_r(r), 0, v_\phi(r))$, and $\mathbf{B} = (B_r(r), 0, B_\phi(r))$ at $\theta = \pi/2$. In addition of course to Ω, we again assume that the following quantities are known at the reference radius: ρ_0, T_0, and B_{r0} (but *not* $B_{\phi 0}$!). We will make use of the polytropic approximation as in chapter 3, but the mathematical treatment of the problem is considerably complicated by the need to (1) include the Lorentz force in the momentum equation, and (2) solve simultaneously an evolution equation for the magnetic field components.

Under the assumptions listed above, the mass conservation equation is still

$$\frac{1}{r^2}\frac{\partial}{\partial r}(r^2\rho v_r) = 0. \tag{4.16}$$

The r and ϕ-components of the equations of motion take the form

$$\rho\left(v_r\frac{\partial v_r}{\partial r} - \frac{v_\phi^2}{r}\right) = -\rho\frac{\partial V}{\partial r} - \frac{\partial p}{\partial r} - \frac{B_\phi}{4\pi\, r}\frac{\partial}{\partial r}(rB_\phi) \tag{4.17}$$

$$\rho\left(v_r\frac{\partial v_\phi}{\partial r} + \frac{v_r v_\phi}{r}\right) = \frac{B_r}{r}\frac{\partial}{\partial r}(rB_\phi) \tag{4.18}$$

The ϕ-component of the induction equation becomes

$$\frac{1}{r}\frac{\partial}{\partial r}(rv_r B_\phi - rv_\phi B_r) = 0, \tag{4.19}$$

while the equation for the r-component is trivially satisfied ($0 = 0$!). A constraint on B_r can however be obtained via the equation $\nabla\cdot\mathbf{B} = 0$:

$$\frac{1}{r^2}\frac{\partial}{\partial r}(r^2 B_r) = 0 \tag{4.20}$$

For $r > 0$, equations (4.16), (4.20) and (4.19) integrate directly to

$$r^2\rho v_r = C_1, \tag{4.21}$$

$$r^2 B_r = C_2, \tag{4.22}$$

$$r(v_r B_\phi - v_\phi B_r) = C_3, \tag{4.23}$$

where C_1, C_2 and C_3 are constants. The first two correspond respectively to the mass flux and magnetic flux associated with the wind. To evaluate the third constant, we transform to a frame co-rotating with the Sun, i.e.

$$v_\phi \to v'_\phi + \Omega r, \tag{4.24}$$

where a primed quantity indicates evaluation in the corotating frame. In the co-rotating frame, $\mathbf{B}$ is stationary, and in view of the perfectly conducting approximation $\mathbf{v}$ and $\mathbf{B}$ are parallel:

$$v'_r/v'_\phi = B'_r/B'_\phi. \tag{4.25}$$

Equation (4.23) then yields

$$C_3 = -\Omega r^2 B_r \tag{4.26}$$

since $B'_r = B_r$. This allows us to rewrite eq. (4.23) as

$$B_\phi = \frac{B_r}{v_r}(v_\phi - \Omega r). \tag{4.27}$$

Equation (4.18) can be rewritten as

$$\frac{\partial}{\partial r}(r v_\phi) = \frac{B_r}{4\pi\rho v_r}\frac{\partial}{\partial r}(r B_\phi) \tag{4.28}$$

But in view of eqs. (4.21) and (4.22), we have $B_r/4\pi\rho v_r = C_2/4\pi C_1$, i.e., a constant! Therefore eq. (4.28) integrates directly to

$$r v_\phi - \frac{r B_\phi B_r}{4\pi\rho v_r} = L, \tag{4.29}$$

where L is another constant, corresponding to the total angular momentum per unit mass carried away by the wind. It has two distinct contributions. The first term on the LHS is the angular momentum associated with the moving fluid element, while the second is the torque density associated with the magnetic field (which is being dragged away by the gas, remember?).

We have already gathered enough information to draw some interesting conclusions about the behavior of the flow. First introduce expressions for the *Alfvén velocities* associated with each component of the magnetic field:

$$A_r = B_r/(4\pi\rho)^{1/2}, \qquad A_\theta = B_\theta/(4\pi\rho)^{1/2}, \qquad A_\phi = B_\phi/(4\pi\rho)^{1/2}. \tag{4.30}$$

Equation (4.27) and (4.29) becomes

$$A_\phi = \frac{A_r}{v_r}(v_\phi - \Omega r), \tag{4.31}$$

$$v_\phi = \frac{L}{r} + \frac{A_r A_\phi}{v_r}. \tag{4.32}$$

Substituting for A_ϕ in (4.32) using (4.29) and (4.30) yields, after some manipulations

$$v_\phi = \Omega r \frac{(v_r^2 L/\Omega r^2) - A_r^2}{v_r^2 - A_r^2}. \tag{4.33}$$

Clearly, if the radial flow velocity ever becomes equal to the radial Alfvén velocity, we are in serious trouble. Unless, of course, the numerator also happens to vanish whenever $v_r = A_r$. Denote the radius at which this occurs (the *Alfvén radius*) as r_A. Then,

$$\left[\frac{v_r^2 L}{\Omega r^2} - A_r^2\right]_{r=r_A} = \frac{A_r^2 L}{\Omega r_A^2} - A_r^2 = 0. \tag{4.34}$$

This is satisfied provided that

$$L = \Omega r_A^2. \tag{4.35}$$

Remember that L is the total angular momentum per unit mass carried away by the wind (cf. eq. [4.29]), i.e., *including* the torque density associated with the magnetic field. Equation (4.35) says that this is equal to the angular momentum that would be carried away by an unmagnetized wind flowing strictly radially ($v_\phi = 0$), and corotating out to a radius r_A. This is an important result !

Lets go back to the r-component of the equations of motion:

$$\rho\left(v_r \frac{\partial u_r}{\partial r} - \frac{v_\phi^2}{r}\right) = \frac{GM_\odot \rho}{r^2} - \frac{\partial p}{\partial r} - \frac{B_\phi}{4\pi\, r}\frac{\partial}{\partial r}(rB_\phi) \tag{4.37}$$

We must work on that a bit. First use eq. (4.27) to substitute for B_ϕ in front of the derivative appearing in the last term on the RHS of eq. (4.37). Then make use of eq. (4.28) to get rid of the B_ϕ derivative that is multiplied by v_ϕ (but not the one multiplied by Ω!). After a bit of straigthforward but tedious algebra and making use of eqs. (4.30) to convert magnetic component to Alfvén velocity components, eq. (4.37) can be cast into the following form:

$$\frac{\partial}{\partial r}\left[\frac{1}{2}(v_r^2 + v_\phi^2) - \frac{GM_\odot}{r} + \frac{c_{s0}^2}{\alpha - 1}\left(\frac{\rho}{\rho_0}\right)^{\alpha-1} - \frac{(\Omega r)A_r A_\phi}{v_r}\right] = 0, \tag{4.38}$$

indicating that the quantity in square brackets is a constant. As the previous wind solutions that we have encountered (§2.2 and 3.1), this constant is the energy per unit mass associated with the flow, which we will again denote by E. Examine carefully eq. (4.38). The only difference with eq. (3.14) lies in the presence of the last term in the square brackets. Note that this term is proportional to the surface rotation rate Ω. Consider then the following situation: a non-rotating configuration, with $A_\phi = 0$ at $t = 0$. Equation (1.17) yields $\partial v_\phi / \partial t = 0$ at all times, so that from eq. (4.27) $B_\phi = 0$ at all times also. Equation (4.38) then becomes identical to eq. (3.4), obtained for a non-rotating, unmagnetized wind. But we have *not* set $B_r = 0$ here! This means that introducing a radial magnetic field component in the Parker solution leaves it unchanged[7,8].

Obtaining a full solution [i.e. $v_r(r)$, $v_\phi(r)$, and so on] is now a much more complicated procedure. The starting point is the manipulation of the r-component of the equations of motion into the form:

$$\frac{\partial v_r}{\partial r} = \left(\frac{v_r}{r}\right) \frac{(v_r^2 - A_r^2)(2c_s^2 + v_\phi^2 - GM_\odot/r) + 2v_r v_\phi A_r A_\phi}{(v_r^2 - A_r^2)(v_r^2 - c_s^2) - v_r^2 A_\phi^2}, \tag{4.39}$$

which involves some straightforward but tedious algebraic manipulations. The RHS of this expression looks like it may blow up for some values of v_r. The denominator actually vanishes when v_r becomes equal to the phase speed of either the fast or slow magnetosonic wave mode[9], which occurs at distinct radial position which we denote r_f and r_s (there is room for confusion here with the sonic point of the Parker solution, which we also denoted r_s. Be careful). Denote by N and D the numerator and denominator on the RHS of eq. (4.39). We require that

$$N(r_f, v_f) = 0, \tag{4.40a}$$

$$D(r_f, v_f) = 0, \tag{4.40b}$$

$$N(r_s, v_s) = 0, \tag{4.40c}$$

$$D(r_s, v_s) = 0, \tag{4.40d}$$

which we complement by the requirements that

$$E(r_f, v_f) = E(v_{r0}, r_0), \tag{4.40e}$$

$$E(r_s, v_s) = E(v_{r0}, r_0), \tag{4.40f}$$

Equations (4.40) are six coupled transcendental equations, which must be solved simultaneously for the elements of the solution 6-vector

$$\mathbf{w} = (v_{r0}, v_{\phi 0}, r_f, v_{rf}, r_s, v_{rs}). \tag{4.41}$$

---

[7] In view of the discussion in §4.1 above, this was to be expected. Or was it?

[8] How about if we have $B_\phi = 0$ and $v_\phi = 0$ at $t = 0$, but a non-vanishing rotation rate Ω? Would this also lead to a solution identical to Parker's solution?

[9] A disgression into the physical nature of the various magnetosonic modes would, at this juncture, take us too far away from our subject matter. These correspond to various ways that "signals" can be transmitted in a magnetized, conducting, compressible fluid, and will actually be discussed in more detail in part III of this course.

You guessed it, this is yet another non-linear root finding problem. With one formidable complication: it is a a 6-D non-linear root finding problem for a set of six coupled non-linear equations. And there are just no good algorithm to solve this kind of root finding problem[10]. We'll have to be a bit creative here; begin by defining a function

$$f(\mathbf{w}) = \Big[N^2(r_f, v_f) + D^2(r_f, v_f) + N^2(r_s, v_s) + D^2(r_s, v_s)$$

$$+(E(r_f, v_f) - E(v_{r0}, r_0))^2 + (E(r_s, v_s) - E(v_{r0}, r_0))^2\Big], \qquad (4.42)$$

so that our root finding problem is now

$$f(\mathbf{w}) = 0, \qquad (4.43)$$

which already looks friendlier, although it must be kept in mind that we have *six* quantities to adjust, as opposed to one, in order to find the root. Clearly $f(\mathbf{w}) > 0$, so that the root finding problem can be cast as a *minimization problem*. And the minimization of a single, nonlinear multidimensional functions is something that is usually easier than a root finding problem for a set of coupled equations. Note that while all roots of eqs. (4.40) will correspond to a minimum (in fact, a zero) of $f(\mathbf{w})$, not all minima of $f(\mathbf{w})$ should be expected to be roots of eqs. (4.40). Clearly, if we want to avoid getting "stuck" in a minimum that is not a zero we will want to have a pretty good starting guess for $\mathbf{w}$. Likewise, the tolerance criterion must be defined with some care. We want of course $f(\mathbf{w}) = 0$ to within some tolerance δ, say, but keeping in mind where eq. (4.42) came from clearly it would also make sense to require that *each* term in f is also zeroed to within δ', with e.g. $\delta' = \delta/6$. To get into multidimensional minimization methods would, at this stage, take us too far away from our subject matter. Chapter 10 of *Numerical Recipes* provides a pretty solid introduction to this subject, and is highly recommended reading in this context. As a further incentive, Problem (4.2) asks you to use the algorithm for the *conjugate gradient method*, listed and explained in §10.6 of *Numerical Recipes*, to construct a WD solution starting from a known solution[11].

---

[10] Section 9.6 of *Numerical Recipes* contains a brief, yet accessible and insightful discussion of why this is the case.

[11] But wait. It would seem that the pseudocode for the Newton-Raphson method could be readily adapted to our multidimensional problem in the following way:

while $\delta \geq \varepsilon$ **do**
  $\mathbf{w} = \mathbf{w}_0 - f(\mathbf{w}_0) \times (\nabla f|_{\mathbf{w}=\mathbf{w}_0})^{-1}$
  $\delta = \|\mathbf{w} - \mathbf{w}_0\|$
  $\mathbf{w}_0 = \mathbf{w}$
enddo

where $\mathbf{w}_0$ is some initial guess for $\mathbf{w}$, and $\|\mathbf{A}\| = (\mathbf{A} \cdot \mathbf{A})^{1/2}$ is the so-called 2-norm. This is the *steepest descent method*. It works, but excessively slowly in some circumstances; see Fig. 10.6.1 in *Numerical Recipes* for an example.

But back to our wind model. The 6-vector $\mathbf{w}$ fully defines our rotating magnetized wind solution[12], together with, of course, the various input quantities which, for convenience, we will group into a 5-vector

$$\mathbf{z} = (\alpha, c_{s0}, v_g, \zeta, \beta), \tag{4.44}$$

where

$$v_g = \left(\frac{2GM_\odot}{r_0}\right)^{1/2} \tag{4.45}$$

is the usual gravitational escape speed, and we have defined the two dimensionless parameters

$$\zeta = \frac{\Omega r_0}{c_{s0}}, \tag{4.46}$$

$$\beta = \frac{A_{r0}}{c_{s0}}. \tag{4.47}$$

measuring the strength of rotational and magnetic effects, respectively.

Figure 4.3 illustrates the topology of the Weber-Davis solution, for input parameters (i.e., $\mathbf{z}$) corresponding to the present-day Sun, and for a rapidly rotating, strongly magnetized Sun (both models have identical α, c_{s0} and v_g). The present-day Sun solution will be discussed in detail in §4.4 below; at this juncture we simply emphasize that

- The topology is a lot more complex than the simple polytropic solutions of §3.1,
- The slow magnetosonic point is the true sonic point for the wind solution,
- Most important, there is one and only one accelerating solution that extend from r_0 to ∞, and this is the one solution that crosses all three critical points. There is no longer any allowed fully subsonic solution.
- Increasing the rotation and magnetic field increases the asymptotic ($r \to \infty$) flow speed by an order of magnitude, but seems to increases the base flow speed by much less (a factor of ~ 3, actually).

You may have guessed that our next task is to reconstruct a full solution, i.e., all velocity and magnetic field components at all r? The first step is to express E as a function of only r, v_r, and the six quantities (v_{r0}, $v_{\phi 0}$, r_s, v_{rs}, r_f, and v_{rf}) solved for previously. This is done in the following way:

[12] But shouldn't our solution also pass through the Alfvén point!? Remember, this is the position r_A at which $v_r = A_r$, and is a critical point of the ϕ-momentum equation (see above). It turns out that any solution going through both critical point of the r-momentum equation *automatically* goes through the Alfvén point. This not-so-obvious characteristic of the WD solution has been studied by Goldreich & Julian (1970, ApJ, 160, 971).

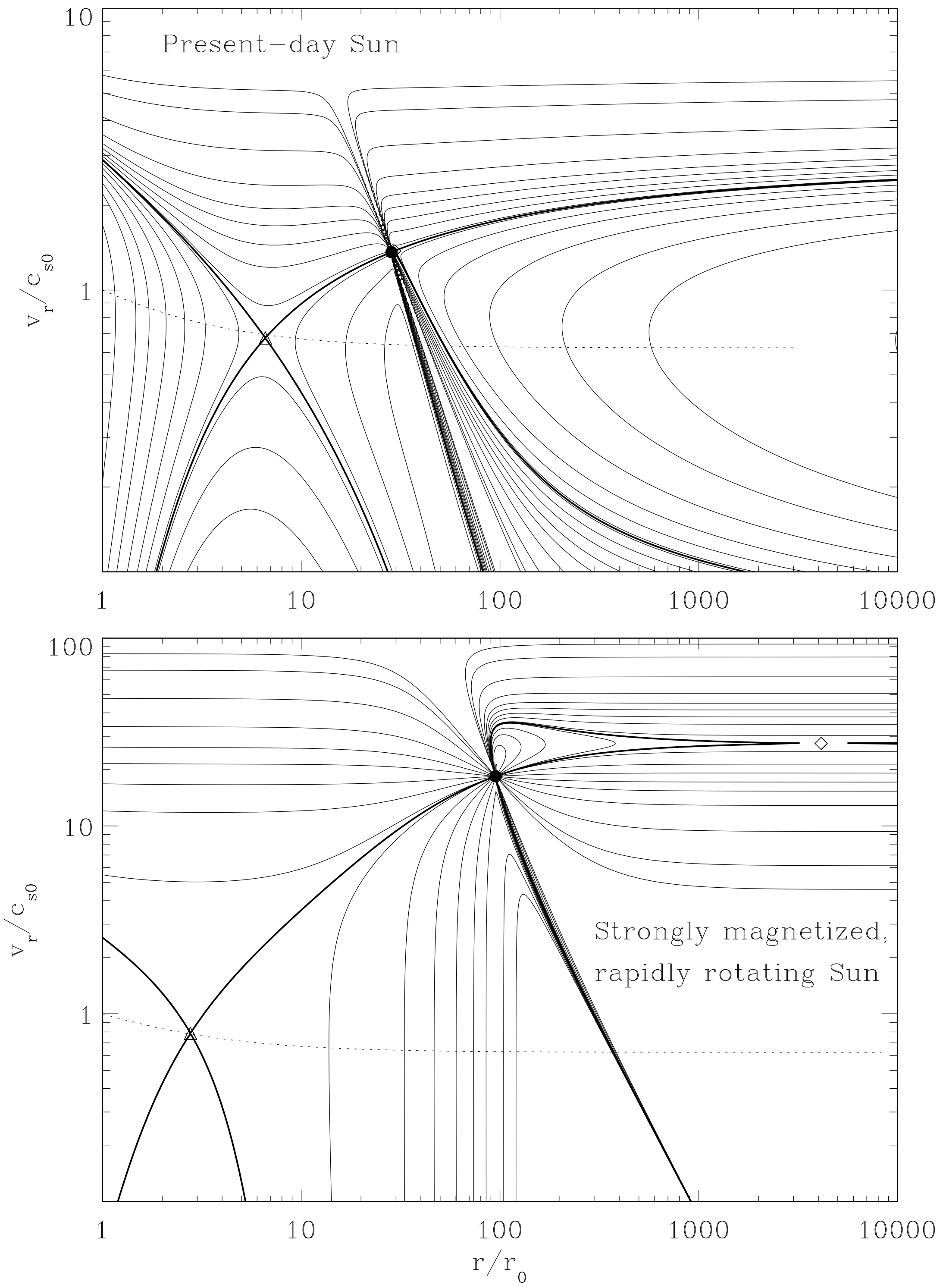

Figure 4.3: Topology of the WD solution for the present day Sun [top] and a strongly magnetized, rapidly rotating Sun (25 times present rotation rate and surface field strength). The triangle, solid dot and diamond are the slow, Alfvén and fast point, respectively (note that the latter two almost coincide in the present-day Sun solution). Note also that the vertical scales differ in both panels.

(1) A_r is a function of B_r and ρ; B_r is only a function of r via eq. (4.22), and ρ of r and v_r via eq. (4.21). So we have $A_r(r, v_r)$.
(2) Using eq. (4.33), v_ϕ can be expressed directly in terms of r and v_r once A_r is known.
(3) B_ϕ (and thus A_ϕ) can then be obtained directly using eq. (4.31). So we have $E(r, v_r)$.

Do we really ? For a given B_0, T_0, ρ_0 and Ω, we can specify everything... except L, required to compute v_ϕ. We cannot use eq. (4.35), since we do not know r_A. But there are other options. Isolating L in eq. (4.32), substituting in for A_ϕ from eq. (4.31) and evaluating everything at r_0 yields

$$L = r_0 v_{\phi 0} \left[1 - \left(\frac{A_{r0}}{v_{r0}} \right)^2 \right] + \Omega r_0^2 \left(\frac{A_{r0}}{v_{r0}} \right)^2 . \tag{4.48}$$

involving only known quantities. So we have $E(r, v_r)$. Equating this expression to $E(r_0, v_{r0})$ leaves us with, yes indeed, a non-linear root finding problem, except that now we are back to out familiar 1-D root finding problem in 1-D, for which the bisection method worked so well... From that point on, $\rho(r)$ is obtained immediately using eq. (4.25), and $A_r(r)$ using eq. (4.26). Then $v_\phi(r)$ is computed using eq. (4.33), after which $A_\phi(r)$ is obtained via eq. (4.31) and we finally have our full solution.

4.4 Yet another comparison to the "real" solar wind

Time to apply the Weber-Davis MHD wind model to the solar wind. The input and solution vectors are

$$\mathbf{z}_\odot = (1.1, 165., 0.01415, 3.495, 3.688) \tag{4.49}$$

$$\mathbf{w}_\odot = (0.0123, 0.0140, 6.60, 0.676, 29.5, 1.378) \tag{4.50}$$

with all distances measured in units of r_0 and velocities in units of the base sound speed c_{s0}. Table 4.1 lists some properties of our WD model, as applied to the solar wind. This is again a solution with $T_0 = 1.5 \times 10^6$ K, $\alpha = 1.1$, and $r_0 = 1.15\, R_\odot$ cm. Clearly, the WD model also does a pretty good job at reproducing the observed properties of low speed streams at 1 AU[13], in the sense that as in the model of §3.4 both the flow speed and particle density are within the observed fluctuations. In addition to the model of §3.4, however, the WD model "predicts" a non-zero value for v_ϕ, which can be translated into a deflection angle (ϕ_v) between the flow direction and the radial direction. The WD model also yields directly a value for the angle ϕ_B between the direction of magnetic fieldlines and the radial direction.

[13] What is the $v_\phi(r)$ predicted by the standard Parker solution ?

Note that the value predicted at 1 AU is only very slightly smaller than that obtained in §4.1[14],

Table 4.1

Properties of the WD wind solution for the present-day Sun

r	v_r [km s^{-1}]	N [cm^{-3}]	T [K]	ϕ_v [deg.]	ϕ_B [deg.]
r_0	2.02	10^8	1.5×10^6	48.7	-0.59
r_s	115	37400	6.8×10^5	4.01	-3.95
r_f	231	891	4.7×10^5	2.00	-15.7
$r_\oplus$	319	17	3.1×10^5	0.53	-54.5
$10\,r_\oplus$	380	0.14	1.9×10^5	0.06	-81.0

Figure 4.4 illustrate the full solution, i.e., the $v_r(r)$, $v_\phi(r)$, $B_r(r)$, $B_\phi(r)$, $\rho(r)$, and $c_s(r)$ profiles, out to $50\,r_0$. The solid dots correspond again to the slow and fast magnetosonic points. Notice how the sound speed is decreasing rather slowly with distance, and that at all distances, $v_\phi \ll v_r$. Clearly, the slow magnetosonic point is the true sonic point ($v_r = c_s$) for this solution[15]. Although both B_r and B_ϕ decrease rapidly with distance, the ratio B_ϕ/B_r, on the other hand, increases rapidly with r close to r_0, but more and more slowly as r increases beyond r_f. Since $r_A \simeq r_f$, we also have that $A_{rA} \simeq c_s$ within a factor of two.

But by and large, our WD wind model predicts flow speeds and densities almost identical to the non-rotating, unmagnetized models of §3.4. Examination of the force balance in the WD wind solution (Fig. 4.4, bottom panel) immediately reveals why this is the case; the magnetic and centrifugal contributions to the net acceleration are, everywhere in the flow, orders of magnitude smaller than the thermal acceleration. The dynamics of the flow are then very much like that characterizing the polytropic wind models of chapter 3. In particular, the expression obtained in §3.2 for the asymptotic flow speed (cf. eq. [3.14]) holds here also.

4.5 Asymptotic behavior

In retrospect, it is almost disappointing how little our solar WD model differed from its non-rotating, unmagnetized polytropic counterpart. This is due, to a large extend, to the relatively low rotation rate of the Sun[16], and to its relatively

[14] Any idea as to why this may be the case ?

[15] Can you imagine how the solution topology transforms smoothly into that of the Parker solution (Fig. 3.1) as $\zeta \to 0$ and $\beta \to 0$? In particular, what happens to the critical points r_s, r_A and r_f ?

[16] "Relatively" because for dynamo modelers, the Sun is actually a fast rotator ! More on this in alater part of this course.

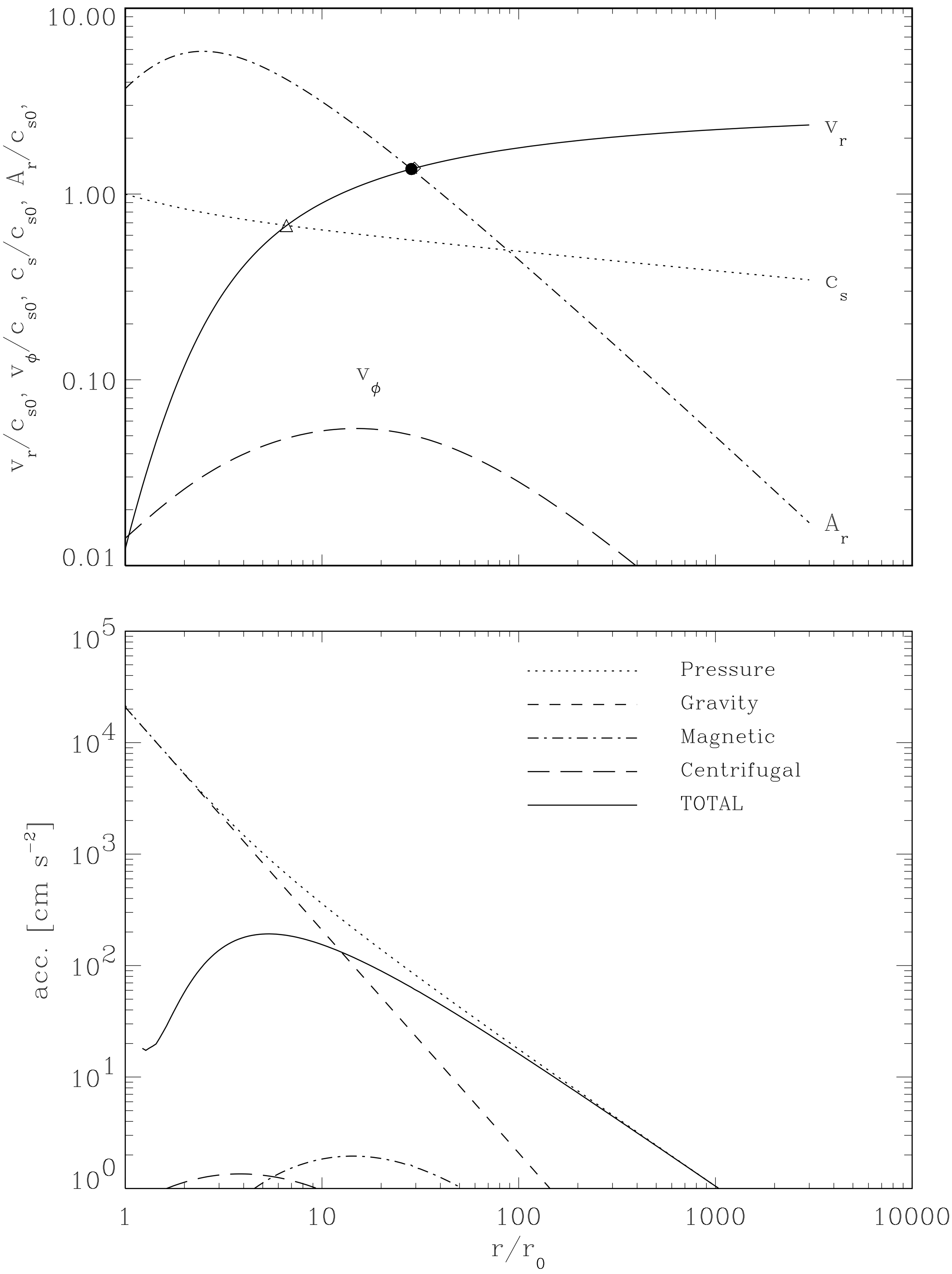

Figure 4.4: The full solution for the WD wind model as applied to the present-day Sun [top], and details of the force balance [bottom]. The solution vector for this solution is $\mathbf{w} = (0.0122947350, 0.0140226022, 6.60039090, 0.676146092, 29.5224232, 1.37785016)$.

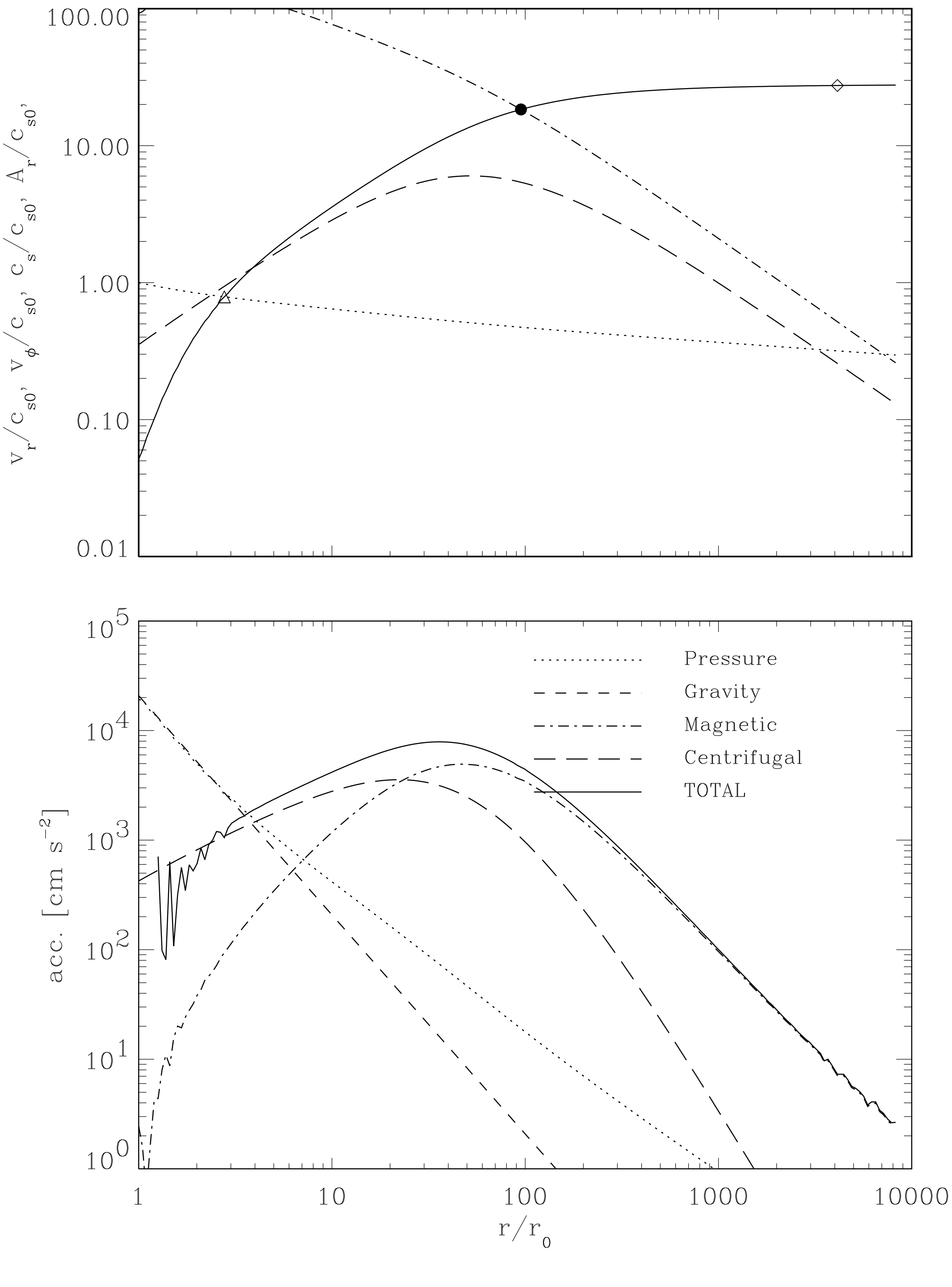

Figure 4.5: Similar to Fig. 4.4, but for a WD solution corresponding to a strongly magnetized ($B_{r0} = 25\,B_{r0,\odot}$), rapidly rotating ($\Omega = 25\,\Omega_\odot$) Sun. The solution vector for this model is $\mathbf{w} = (0.0511436117, 0.352765862, 2.77375964, 0.786555424, 4127.64854, 27.5026241)$. Note how the magnetic tension force is now the prime contributor to the wind's acceleration at large distances.

low magnetic field strength (by which, incidentally, we refer to the global solar magnetic field outside of active regions). Figure 4.5 shows a WD model for a "Sun" rotating at 25 times its present angular velocity, with a corresponding increase in its magnetic field strength[17]. We have again assumed $\alpha = 1.1$ and $T_0 = 1.5 \times 10^6$ K. Clearly there are now drastic differences with the models of chapter 3. The asymptotic flow speed now exceeds the local sound speed by nearly two orders of magnitudes. That's a Mach 10^2 flow we have here ! The azimuthal velocity v_ϕ now exceeds the radial flow speed within the sonic point, and remains comparable to it out to the Alfvén point. These dramatic differences can be traced directly to the effects of the centrifugal and magnetic contributions to the net acceleration (Fig. 4.5, bottom panel). While the flow remains motsly thermally driven near the coronal base, within a few r_0 the centrifugal and magnetic terms become comparable to the thermal pressure term, and completely dominate the dynamics of the flow thereafter. At asymptotically large distances, the flow is in fact being driven almost exclusively by the magnetic force. It can be shown (try it!) that the asymptotic flow speed is now

$$\lim_{r\to\infty} v_r \equiv v_{r\infty} \simeq \left(\frac{\Omega^2 r_0^4 B_{r0}^2}{\dot{\mathrm{M}}}\right)^{1/3}, \tag{4.49}$$

with $\dot{\mathrm{M}} = 4\pi\rho_0 r_0^2 v_{r0}$ as in §2.2. Figure 4.6 shows the variations with distances of the two contributions to the total angular momentum carried away by the wind [see eq. (4.29)]. The solid line is the specific angular momentum carried away by the gas, and the dashed line is the torque density associated with the magnetic field. Note how the latter is more than one order of magnitude larger than the former. As advertised previously, the sum of these two contributions (dotted line) is a constant. Note that the rapidly rotating, strongly magnetized wind carries *a lot* more angular momentum than its solar-type counterpart. In view of eq. (4.35) one may have expected a factor of 25 difference or something like that, but variations in the position of the Alfvén point conspire to lead to an even larger angular momentum loss rate; one can (relatively) easily show that in the limit of weak centrifugal and magnetic driving (cf. the solar case of Fig. 4.4),

$$r_A \simeq \frac{r_0^2 B_{r0}}{(\dot{\mathrm{M}} v_{r\infty})^{1/2}}, \tag{4.50}$$

as opposed to

$$r_A \simeq \left(\frac{3}{2}\right)^{1/2} \left(\frac{v_{r\infty}}{\Omega}\right), \tag{4.51}$$

[17] We are getting ahead of ourselves again a bit here; simple (some would say simplistic) dynamo models predict (sort of) that for rotation rates of the order of the Sun's, the strength of the dynamo-generated magnetic field increases linearly with the rotation rate.

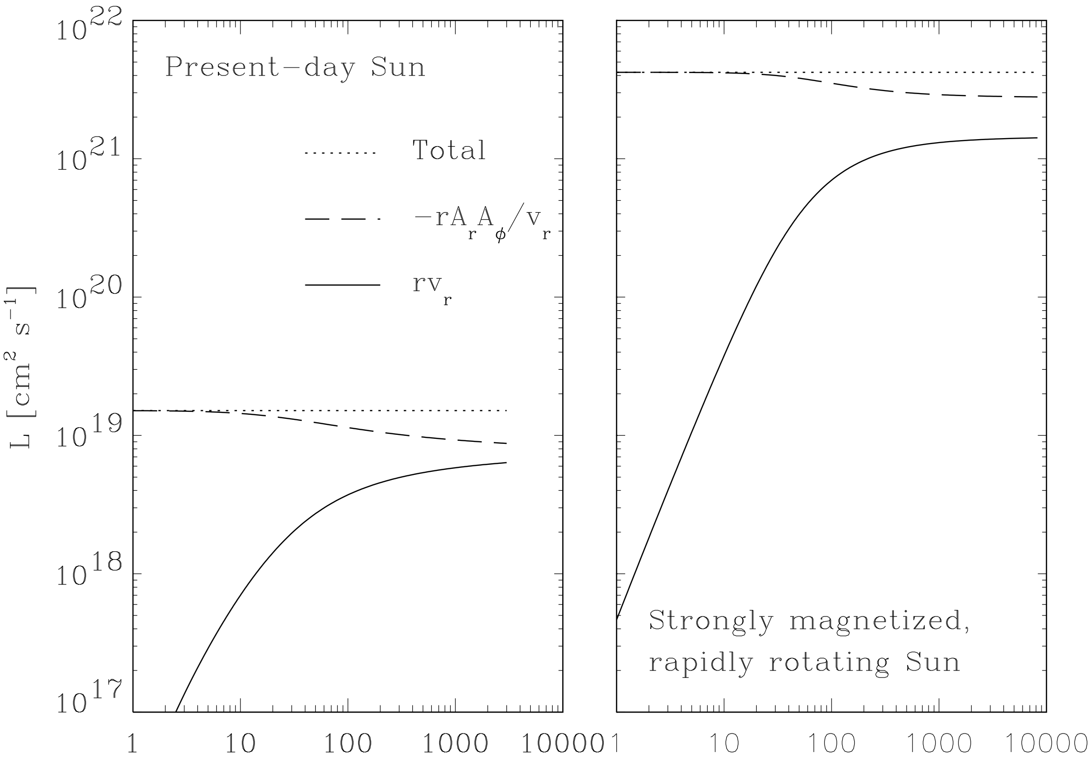

Figure 4.6: Contributions to the total angular momentum carried away by the wind. The solid line is the (usual) angular momentum per unit mass, and the dashed line the torque density associated with the deformed magnetic field. The sum of these two contributions (dotted line), the total wind specific angular momentum, is a constant of the motion [cf. eq. (4.29)].

for the rapidly rotating, strongly magnetized model of Fig. 4.5.

4.6 Effects of mass loss on solar structure and rotation

Knowing v_{r0} allows us to compute the mass loss rate (cf. eq. [2.19]). For the solution of Fig. 4.4, one obtains

$$\dot{\mathrm{M}}_\odot = 2.4 \times 10^{-14} \mathrm{M}_\odot \, \mathrm{yr}^{-1}. \tag{4.52}$$

This result assumes implicitely that our solution is valid over the whole sphere, which is likely not the case[18], so that the above estimate is likely uncertain by a factor of order unity. It does, however, fits rather nicely the observationally determined solar mass loss rate[19]. For the "young Sun" of Figure 4.5, this goes up by a

[18] Why is it not the case here ?

[19] There's a catch of cosmic proportion here; the "observationally determined mass loss rate" is estimated by measuring the mass flux at 1 AU... and assuming that this mass flux is independent of latitude ! This unfortunate state of affairs is however changing with the probe *Ulysses*.

mere factor of four. Now mass loss can influence internal structure (and evolution) to a significant degree. However, at a mass loss rate $\dot{\mathrm{M}}_\odot \sim 10^{-14}\mathrm{M}_\odot\,\mathrm{yr}^{-1}$, the Sun will lose, over the course of its evolution on the main sequence, a total mass fraction

$$\frac{\Delta M_\odot}{M_\odot} = \frac{\dot{\mathrm{M}}_\odot \times \tau_{\mathrm{MS}}}{M_\odot} \simeq 10^{-4}, \tag{4.53}$$

for a main-sequence lifetime $\tau_{\mathrm{MS}} = 10^{10}\,\mathrm{yr}$. This is too small to cause significant structural change in the solar interior[20].

Problems

(4.1) Using the input and solution vectors listed in the caption to Figure 4.4, reconstruct the full WD solution, following the procedure outlined in the text. Construct a non-rotating, non-magnetized polytropic solution with the same α and T_0 (for example following the procedure outlined in §3.1). Compare the shape of both magnetic field spirals.

(4.2) Using as a starting guess the solution vector for the present-day sun WD wind solution, use the conjugate gradient method (listing in *Numerical Recipes*, see text) to construct a new solution vector for *either*

(a) A coronal base temperature of $T_0 = 2 \times 10^6\,\mathrm{K}$,
(b) $\Omega = 2 \times \Omega_\odot$,
(c) $B_r = 2 \times B_{r\odot}$.

Whichever one you choose, keep all other physical input quantities identical to the basic present-day Sun solution of §4.4.

[20] While this may be the case for the Sun, mass loss has a strong influence on the evolution of massive stars ($M_* \gtrsim 10 M_\odot$), mostly because their winds carries a much larger mass flux. Can you think of a reason why the mass loss is larger in these objects ?

Bibliography

The extension of the Sun's magnetic field into interplanetary space by the solar wind is most clearly described in

Parker, E.N. 1963, *Interplanetary Dynamical Processes* (New York: John Wiley), chap. 10.

The original paper by Weber and Davis is

Weber, E.J., & Davis, L. Jr 1967, ApJ, 148, 217,

but the following paper is not to be missed:

Belcher, J.W., & MacGregor, K.B. 1976, ApJ, 210, 498.

The confrontation of the WD model with observations is discussed critically in

Pizzo, V., Schwenn, R., Marsch, E., Rosenbauer, H., Mülhäuser, K.-H., & Neubauer, F.M. 1983, ApJ, 271, 335.

An application of the WD model to protostellar objects can be found in

Hartmann, L., & MacGregor, K.B. 1982, ApJ, 259, 180,

while the extension to hot stars, including radiation forces, was carried out by

Friend, D.B., & MacGregor, K.B. 1984, ApJ, 282, 591.

The failure of WD-type solutions to satisfy force balance in the θ-direction, and the potential consequences of such a failure, are investigated in

Suess, S.T., & Nerney, S.F. 1973, ApJ, 184, 17,
Nerney, S.F., & Suess, S.T. 1975, ApJ, 196, 837.

Truly consistent extension of the WD formalism out of the equatorial plane are exceedingly rare. The following is noteworthy

Sakurai, T. 1985, MNRAS, 152, 121.

A different approach that has received considerable attention consists in constructing approximation to the MHD equations, while retaining realistic field geometries, etc. These are useful in providing order-of-magnitude estimates of a number of geometrically-related effects omitted in the WD model. See the following

Mestel, L. 1968, MNRAS, 138, 359.
Collier Cameron, A., Jianke, L., & Mestel, L. 1990, in *Angular Momentum Evolution of Young Stars*, eds. S. Catalano & J.R. Stauffer (Dordrecht: Kluwer), p. 297.